View metadata, citation and similar papers at core.ac.uk

brought to you by CORE

provided by Haverford College: Haverford Scholarship

Haverford College

Haverford Scholarship

Faculty Publications

Physics

2003

The Parkes Multibeam Pulsar Survey - III. Young Pulsars and the Discovery and Timing of 200 Pulsars

M. Kramer

J. F. Bell

R. N. Manchester

A. G. Lyne

Fronefield Crawford
Haverford College, fcrawford@haverford.edu

Follow this and additional works at: https://scholarship.haverford.edu/physics_facpubs

Repository Citation

"The Parkes Multibeam Pulsar Survey - III. Young Pulsars and the Discovery and Timing of 200 Pulsars" M. Kramer, J. F. Bell, R. N. Manchester, A. G. Lyne, F. Camilo, I. H. Stairs, N. D'Amico, V. M. Kaspi, G. Hobbs, D. J. Morris, F. Crawford, A. Possenti, B. C. Joshi, M. A. McLaughlin, D. R. Lorimer, & A. J. Faulkner, Monthly Notices of the Royal Astronomical Society, 342, 1299 (2003).

This Journal Article is brought to you for free and open access by the Physics at Haverford Scholarship. It has been accepted for inclusion in Faculty Publications by an authorized administrator of Haverford Scholarship. For more information, please contact nmedeiro@haverford.edu.

Mon. Not. R. Astron. Soc. **342,** 1299–1324 (2003)

The Parkes Multibeam Pulsar Survey – III. Young pulsars and the discovery and timing of 200 pulsars

M. Kramer,[1⋆] J. F. Bell,[2] R. N. Manchester,[2] A. G. Lyne,[1] F. Camilo,[3] I. H. Stairs,[4] N. D'Amico,[5,6] V. M. Kaspi,[7] G. Hobbs,[1,2] D. J. Morris,[1] F. Crawford,[8] A. Possenti,[6,9] B. C. Joshi,[1,10] M. A. McLaughlin,[1] D. R. Lorimer[1] and A. J. Faulkner[1]

[1]*University of Manchester, Jodrell Bank Observatory, Macclesfield, Cheshire SK11 9DL*
[2]*Australia Telescope National Facility, CSIRO, PO Box 76, Epping NSW 1710, Australia*
[3]*Columbia Astrophysics Laboratory, Columbia University, 550 West 120th Street, New York, NY 10027, USA*
[4]*Department of Physics & Astronomy, University of British Columbia, 6224 Agricultural Road, Vancouver, BC, Canada V6T 1Z1*
[5]*Dipartimento di Fisica, Università di Cagliari, SP Monserrato-Sestu Km 0.700, I-09042 Monserrato, Italy*
[6]*Osservatorio Astronomico di Cagliari, loc. Poggio dei Pini, Strada 54, I-09012 Capoterra, Italy*
[7]*McGill University, 3600 University St, Montreal, Quebec, Canada H3T 2A8*
[8]*Department of Physics, Haverford College, Haverford, PA 19041, USA*
[9]*Osservatorio Astronomico di Bologna, via Ranzani 1, I-40127 Bologna, Italy*
[10]*National Center for Radio Astrophysics, PO Bag 3, Ganeshkhind, Pune 411003, India*

Accepted 2003 March 14. Received 2003 March 14; in original form 2002 November 29

ABSTRACT

The Parkes Multibeam Pulsar Survey has unlocked vast areas of the Galactic plane, which were previously invisible to earlier low-frequency and less-sensitive surveys. The survey has discovered more than 600 new pulsars so far, including many that are young and exotic. In this paper we report the discovery of 200 pulsars for which we present positional and spin-down parameters, dispersion measures, flux densities and pulse profiles. A large number of these new pulsars are young and energetic, and we review possible associations of γ-ray sources with the sample of about 1300 pulsars for which timing solutions are known. Based on a statistical analysis, we estimate that about 19 ± 6 associations are genuine. The survey has also discovered 12 pulsars with spin properties similar to those of the Vela pulsar, nearly doubling the known population of such neutron stars. Studying the properties of all known 'Vela-like' pulsars, we find their radio luminosities to be similar to normal pulsars, implying that they are very inefficient radio sources. Finally, we review the use of the newly discovered pulsars as Galactic probes and discuss the implications of the new NE2001 Galactic electron density model for the determination of pulsar distances and luminosities.

Key words: pulsars: general – ISM: structure – Galaxy: structure – gamma-rays: observations.

1 INTRODUCTION

We increase our understanding of pulsars by studying them as a population or by studying specific and/or exotic examples such as binary, millisecond, young or glitching pulsars. The Parkes Multibeam Pulsar Survey (hereafter PMPS) set out to find a large number of pulsars previously hidden from past surveys performed at low frequencies and/or with short integration times. Distant pulsars in the Galactic plane that were previously undetectable due to scattering and dispersion broadening of their signals propagating through the interstellar medium were expected to be found in large numbers. Among the new pulsars, a few exotic systems should be present, and the discovery of pulsars in remote parts of the Galaxy promised to provide a unique opportunity for population studies and the understanding of the Galaxy.

The PMPS has fulfilled all of these promises. It has found a large number of young (e.g. Camilo et al. 2000; D'Amico et al. 2001), distant (this work), exotic (Lyne et al. 2000; Kaspi et al. 2000b; Camilo et al. 2001b; Stairs et al. 2001) and glitching pulsars (Hobbs et al. 2002) buried in the inner Galactic plane ($|b| < 5^\circ$, $-100^\circ < l < 50^\circ$).

All planned survey pointings have been completed and the first processing of the data has yielded more than 600 newly detected pulsars. Currently, reprocessing with refined software and an accelerated search is underway (Faulkner et al. 2003). By the time reprocessing is completed, the PMPS will have roughly doubled

⋆E-mail: mkramer@jb.man.ac.uk

© 2003 RAS

the number of known pulsars and opened up vast portions of the Galaxy that were previously devoid of known pulsars. A detailed description of the survey including the motivation, telescope, hardware and software details, and the first 220 pulsars discovered were reported by Manchester et al. (2001) and Morris et al. (2002), hereafter Paper I and Paper II, respectively. Many of the more exotic pulsars have been reported separately as noted above. All pulsars with known timing solutions can be found in the on-line catalogue hosted by the ATNF.[1]

In summary, an operating frequency of 1374 MHz minimized the harmful effects of dispersion and scattering that inhibit lower-frequency surveys of this region of the Galaxy. The survey has a limiting sensitivity of about 0.2 mJy (Paper I), far surpassing that of previous wide-area pulsar surveys. This has been made possible by the 13-beam receiver system (Staveley-Smith et al. 1996), which enables this area of sky to be covered in a manageable time.

In Section 2 we report the discovery of 200 new pulsars and catalogue many of their basic parameters obtained after, at least, 1 year of timing observations. We then review in Section 3 the sample of young pulsars, including the large number discovered in this survey. We study their possible associations with γ-ray sources (Section 3.1), using distance estimates of the new 'NE2001' Galactic electron density model (Cordes & Lazio 2002). We then summarize the properties of 'Vela-like' pulsars (Section 3.2), before we comment on the implications of the NE2001 model for the Galactic distribution of pulsars (Section 4).

2 DISCOVERY AND TIMING OF 200 PULSARS

The observation and analysis strategies used are identical to those outlined in Papers I and II. Table 1 lists the pulsar name, the J2000 right ascension and declination from the timing solution, the corresponding Galactic coordinates, the beam in which the pulsar was detected, the radial distance of the pulsar from the beam centre in units of the beam radius (approximately 7 arcmin), the signal-to-noise ratio of the discovery observation from the final time-domain folding in the search process, the mean flux density averaged over all observations included in the timing solution, and pulse widths at 50 and 10 per cent of the peak of the mean pulse profile. The 10 per cent width is not measurable for pulsars with mean profiles having poor signal-to-noise ratio. Estimated uncertainties, where relevant, are given in parentheses where relevant and refer to the last quoted digit. Flux densities may be somewhat overestimated for very weak pulsars or those that have extended null periods, since non-detections are not included in the timing solution. Table 2 gives solar-system barycentric pulse periods, period derivatives, epoch of the period, the number of times of arrival (TOAs) used in the timing solution, the final rms timing residual and the dispersion measure (DM).

For a few pulsars, the timing solutions include data obtained with the 76-m Lovell telescope at Jodrell Bank Observatory. Details of these observations can be found in Paper II. Corresponding sources are marked in Table 1. The table also includes one binary pulsar, PSR J1141−6545. Binary parameters can be found in Kaspi et al. (2000b). Three pulsars, PSRs J1301−6310, J1702−4128 and J1702−4310, showed significant timing noise which was removed, to first order, by fitting a second period derivative to the data. These pulsars are indicated in Table 2.

Table 3 lists derived parameters for the 200 pulsars. After the name, the first three columns give the base-10 logarithm of the characteristic age, $\tau_c = P/(2\dot{P})$ in years, the surface dipole magnetic field strength, $B_s = 3.2 \times 10^{19}(P\dot{P})^{1/2}$ in gauss and the rate of loss of rotational energy, $\dot{E} = 4\pi^2 I \dot{P} P^{-3}$ in erg s^{-1}, where a neutron-star moment of inertia $I = 10^{45}$ g cm^2 is assumed. The next two columns give the pulsar distance d, computed from the DM assuming the Taylor & Cordes (1993, hereafter TC93) model for the Galactic distribution of free electrons and the implied Galactic z distance. Although distances are quoted to 0.1 kpc, in fact they are generally more uncertain than that (typically around 30 per cent) owing to uncertainties in the electron density model. This is especially so for pulsars with very large DMs, indicating large distances from the Sun. Despite the availability of the improved NE2001 model, we use the TC93 model in order to be consistent with Papers I and II where the previous model has been employed. We discuss the uncertainties of the TC93 distances and the difference of both models in more detail in Section 4, when we compare the TC93 values with those inferred from the new NE2001 model.

We use the TC93-model distance to compute the listed radio luminosity, $L_{1400} \equiv S_{1400}d^2$. For a radio spectral index of -1.7 (Maron et al. 2000), these numbers may be converted to the more commonly quoted 400-MHz luminosity by multiplying by 8.4. The majority of all presented measured and derived parameters have already been included in the statistical analyses presented in Paper II.

Mean pulse profiles at 1374 MHz for the 200 pulsars are given in Fig. 1. These profiles were formed by adding all data used for the timing solution. Typically they contain several hours of effective integration time.

3 YOUNG PULSARS

One of the main aims of the PMPS was to find young pulsars. Here we define 'young pulsars' as those with a characteristic age less than 100 kyr. This age is commonly chosen as a cut-off as it includes most pulsars that are likely to glitch often and/or to be associated with supernova remnants (SNRs).

As already demonstrated in Paper II, the strategy of searching the region close to the Galactic plane at high frequencies has indeed been very successful in finding young pulsars: the survey has discovered 39 out of 79 currently known pulsars with $\tau_c \lesssim 100$ kyr.

This newly increased sample of young pulsars is important in studies of the birth properties of radio pulsars, such as the initial spin period, their luminosity, and the kick velocity imparted by asymmetric supernova explosions. Young pulsars also provide a possible origin for many of the previously unidentified point sources detected by the Energetic Gamma Ray Experiment Telescope (EGRET) as has been addressed by many authors (e.g. Merck et al. 1996). A distinct group of young pulsars is that of energetic objects with spin parameters similar to Vela, which may be more typical of the young pulsar population than the Crab pulsar which is unique in several aspects. In the following, we will review the current sample of potential EGRET counterparts and such Vela-like pulsars.

3.1 Pulsar/EGRET source associations

The true nature of the 100 or so unidentified EGRET sources in the Galactic plane has been debated for some time (e.g. Hartman et al. 1999). Pulsars are good candidates because they have a similar spatial distribution and are one of the only two populations of astronomical objects positively identified as being γ-ray emitters, as demonstrated clearly by the Crab and the Vela pulsars. A few recently discovered young pulsars (see below) discovered in this survey have already been plausibly associated with EGRET sources

[1] http://www.atnf.csiro.au/research/pulsar/catalogue/

Table 1. Positions, flux densities and widths for 200 pulsars discovered in the Parkes Multibeam Pulsar Survey. All pulsars were timed using the Parkes telescope. 'J' indicates pulsars that have also been timed at Jodrell Bank. Radial angular distances are given in units of beam radii.

PSR J	RA (J2000) (h m s)	Dec. (J2000) (° ′ ″)	l (deg)	b (deg)	Beam	Radial dist.	S/N ratio	S_{1400} (mJy)	W_{50} (ms)	W_{10} (ms)
0831−4406	08:31:32.43 (3)	−44:06:11.9 (4)	262.29	−2.69	6	0.85	54.9	0.43 (5)	6.1	17
0834−4159	08:34:16.3 (1)	−41:59:51 (1)	260.89	−1.04	3	0.43	25.6	0.19 (3)	5.8	–
0855−4644	08:55:36.18 (3)	−46:44:13.4 (5)	266.97	−1.00	3	0.25	15.6	0.20 (3)	7.5	–
0855−4658	08:55:19.57 (5)	−46:58:22.6 (9)	267.12	−1.19	7	0.19	39.7	0.23 (3)	11.0	22
0945−4833	09:45:38.254 (6)	−48:33:14.50 (5)	274.20	+3.67	5	0.51	39.5	0.39 (5)	4.6	11
1000−5149	10:00:28.141 (6)	−51:49:58.12 (7)	278.11	+2.60	8	1.34	31.0	0.26 (4)	4.5	9
1012−5830	10:12:54.9 (1)	−58:30:25.6 (8)	283.46	−1.76	9	0.82	13.0	0.08 (2)	31	–
1013−5934	10:13:31.854 (6)	−59:34:26.7 (1)	284.13	−2.60	7	0.85	137.6	1.9 (2)	7.4	39
1015−5719	10:15:37.96 (4)	−57:19:12.8 (2)	283.09	−0.58	11	0.61	65.0	0.90 (10)	46	57
1019−5749	10:19:52.14 (4)	−57:49:05.9 (5)	283.84	−0.68	11	1.31	21.9	0.80 (9)	44	–
1020−5921	10:20:14.03 (8)	−59:21:34 (1)	284.72	−1.94	4	0.86	43.9	0.45 (6)	19.0	36
1022−5813	10:22:28.1 (2)	−58:13:30 (4)	284.35	−0.83	4	0.61	19.7	0.20 (3)	36	–
1031−6117	10:31:02.24 (7)	−61:17:50.6 (3)	286.88	−2.88	10	0.73	12.0	0.12 (2)	10.0	–
1035−6345	10:35:03.08 (1)	−63:45:18.41 (6)	288.53	−4.77	6	1.07	20.9	0.24 (3)	8.2	14
1043−6116	10:43:55.29 (3)	−61:16:50.8 (2)	288.22	−2.11	2	1.33	52.1	0.91 (10)	7.0	14
1052−5954	10:52:38.11 (7)	−59:54:44.1 (5)	288.55	−0.40	1	0.42	13.3	0.15 (3)	11.0	–
1054−5943	10:54:57.75 (4)	−59:43:14.1 (5)	288.73	−0.10	4	0.87	52.0	0.31 (4)	4.8	9
1055−6236	10:55:54.61 (7)	−62:36:48.3 (4)	290.08	−2.66	6	0.26	18.6	0.12 (2)	7.3	14
1058−5957	10:58:34.25 (3)	−59:57:36.4 (3)	289.24	−0.12	9	0.90	38.3	0.51 (6)	16.0	23
1103−6025	11:03:31.48 (2)	−60:25:36.39 (9)	289.99	−0.29	2	0.83	33.0	0.17 (3)	5.5	10
1107−6143	11:07:12.3 (2)	−61:43:59 (3)	290.92	−1.32	11	0.83	40.7	0.38 (5)	26	50
1117−6154	11:17:23.81 (9)	−61:54:22 (1)	292.10	−1.03	4	1.16	57.8	0.68 (8)	8.9	30
1117−6447	11:17:45.0 (4)	−64:47:58 (2)	293.17	−3.72	9	0.74	10.1	0.14 (2)	61	–
1124−5638	11:24:56.47 (6)	−56:38:39.7 (5)	291.21	+4.25	11	1.05	15.3	0.31 (4)	15.0	–
1124−6421	11:24:59.5 (1)	−64:21:17 (1)	293.75	−3.04	1	0.86	21.7	0.19 (3)	13.0	–
1128−6219	11:28:46.7 (2)	−62:19:09 (2)	293.50	−0.97	1	0.94	11.0	0.27 (4)	93	–
1130−5826	11:30:16.33 (3)	−58:26:02.3 (3)	292.46	+2.78	9	0.96	22.8	0.18 (3)	4.0	7
1132−5627	11:32:15.74 (4)	−56:27:28.9 (7)	292.11	+4.74	5	0.94	9.2	0.09 (2)	4.9	–
1141−6545	11:41:07.053 (15)	−65:45:18.85 (10)	295.79	−3.86	6	0.55	180.9	3.3 (5)	4.4	14
1148−6415	11:48:37.8 (5)	−64:15:33 (3)	296.18	−2.21	9	0.17	12.4	0.06 (2)	37	–
1152−6012	11:52:53.8 (1)	−60:12:21 (1)	295.72	+1.84	9	1.66	20.7	0.17 (3)	9.6	–
1154−6250	11:54:20.1 (1)	−62:50:02.7 (7)	296.47	−0.68	6	0.70	10.5	0.07 (2)	5.9	–
1159−6409	11:59:21.7 (1)	−64:09:57 (1)	297.30	−1.87	11	1.13	24.6	0.47 (6)	210	–
1201−6306	12:01:23.0 (1)	−63:06:59.5 (8)	297.31	−0.79	9	0.91	10.6	0.13 (2)	13.0	–
1211−6324	12:11:24.18 (7)	−63:24:45.2 (5)	298.47	−0.89	10	0.89	18.4	0.45 (6)	15.0	24
1214−5830	12:14:08.42 (2)	−58:30:25.9 (1)	298.06	+4.01	4	1.32	24.2	0.14 (2)	9.4	18
1222−5738	12:22:52.3 (3)	−57:38:20 (1)	299.10	+5.02	4	1.15	12.9	0.11 (2)	28	–
1225−6035	12:25:28.63 (5)	−60:35:37.6 (3)	299.75	+2.12	13	0.77	26.8	0.26 (4)	3.9	19
1231−6303	12:31:13.0 (3)	−63:03:18 (2)	300.64	−0.27	1	0.62	113.1	1.50 (16)	185	–
1233−6312	12:33:31.5 (9)	−63:12:29 (5)	300.91	−0.41	4	0.64	23.8	0.25 (4)	57	–
1233−6344	12:33:39.9 (1)	−63:44:55 (1)	300.97	−0.94	9	1.03	10.2	0.07 (2)	12.0	–
1235−6354	12:35:57.72 (8)	−63:54:30.4 (4)	301.23	−1.09	8	0.67	14.5	0.16 (3)	10.0	–
1237−6725	12:37:25.9 (1)	−67:25:33.9 (6)	301.58	−4.59	13	1.14	24.4	0.36 (5)	32	47
1243−5735	12:43:35.38 (7)	−57:35:42.8 (5)	301.88	+5.26	1	0.18	18.7	0.14 (2)	12.0	74
1248−6344	12:48:46.36 (5)	−63:44:09.6 (5)	302.64	−0.87	5	0.56	11.0	0.12 (2)	12.0	–
1249−6507	12:49:54.32 (9)	−65:07:19.8 (7)	302.77	−2.25	1	0.52	13.5	0.10 (2)	11.0	–
1254−6150	12:54:32.48 (6)	−61:50:50.8 (3)	303.30	+1.02	1	1.08	10.1	0.15 (3)	3.5	–
1255−6131	12:55:54.86 (4)	−61:31:10.1 (4)	303.47	+1.35	1	0.99	15.9	0.13 (2)	8.6	21
1301−6310	13:01:28.30 (7)	−63:10:40.5 (5)	304.06	−0.33	10	0.58	13.4	0.11 (2)	11.0	–
1302−6313	13:02:19.2 (7)	−63:13:29 (4)	304.16	−0.38	8	0.49	13.5	0.18 (3)	93	–
1306−6242	13:06:44.6 (1)	−62:42:03 (1)	304.69	+0.12	7	1.02	9.1	0.14 (2)	33	–
1309−6526	13:09:00.29 (8)	−65:26:16.6 (5)	304.76	−2.63	5	0.64	11.6	0.15 (3)	10.0	–
1314−6101	13:14:23.4 (9)	−61:01:16 (6)	305.71	+1.73	2	0.93	46.2	0.41 (5)	59	86
1319−6105	13:19:26.32 (2)	−61:05:26.2 (1)	306.31	+1.60	1	1.78	16.1	0.84 (9)	13.0	26
1322−6329	13:22:18.0 (2)	−63:29:37 (2)	306.37	−0.83	7	0.39	13.3	0.17 (3)	34	–
1324−6146	13:24:43.9 (5)	−61:46:00 (3)	306.86	+0.85	12	0.55	44.0	0.73 (8)	72	–
1324−6302	13:24:13.65 (7)	−63:02:21.1 (6)	306.64	−0.40	1	0.64	21.1	0.23 (3)	18.0	–
1329−6158	13:29:03.3 (6)	−61:58:59 (6)	307.33	+0.57	6	0.41	24.9	0.22 (3)	31	–

Table 1 – *continued*

PSR J	RA (J2000) (h m s)	Dec. (J2000) (° ′ ″)	l (deg)	b (deg)	Beam	Radial dist.	S/N ratio	S_{1400} (mJy)	W_{50} (ms)	W_{10} (ms)
1339−6618	13:39:56.6 (2)	−66:18:07.8 (7)	307.79	−3.89	6	0.66	18.7	0.23 (3)	26	–
1344−6059	13:44:39.6 (3)	−60:59:31 (3)	309.34	+1.22	10	0.33	16.1	0.19 (3)	29	–
1354−6249	13:54:35 (1)	−62:49:30 (7)	310.07	−0.83	3	0.33	26.2	0.24 (3)	57	–
1355−5925	13:55:59.11 (5)	−59:25:00.9 (3)	311.07	+2.43	8	0.88	26.5	0.55 (7)	21	43
1355−6206	13:55:21.34 (6)	−62:06:20.1 (5)	310.33	−0.16	8	0.67	22.7	0.54 (6)	19.0	–
1403−6310	14:03:14.0 (2)	−63:10:27 (1)	310.93	−1.42	7	1.43	25.9	0.65 (7)	18.0	33
1406−5806	14:06:01.2 (2)	−58:06:32 (1)	312.67	+3.35	11	0.81	36.2	0.84 (9)	49	–
1413−6141	14:13:09.87 (9)	−61:41:13 (1)	312.46	−0.34	2	0.87	15.2	0.61 (7)	37	–
1418−5945	14:18:32.3 (4)	−59:45:00 (3)	313.71	+1.29	3	0.86	12.5	0.18 (3)	64	–
1420−6048	14:20:08.237 (16)	−60:48:16.43 (15)	313.54	+0.23	11	0.48	36.5	0.91 (10)	8.3	16
1424−5822	14:24:32.11 (3)	−58:22:56.0 (2)	314.90	+2.31	2	1.22	49.8	1.10 (12)	12.0	22
1424−6438	14:24:59.2 (2)	−64:38:10.0 (9)	312.74	−3.56	12	0.95	20.0	0.24 (3)	68	–
1425−5723	14:25:36.56 (3)	−57:23:30.8 (4)	315.38	+3.19	12	0.75	17.2	0.24 (3)	7.1	135
1425−5759	14:25:59.11 (7)	−57:59:10.2 (9)	315.22	+2.61	3	0.94	11.7	0.09 (2)	9.6	–
1434−6006	14:34:05.3 (2)	−60:06:29.0 (9)	315.40	+0.26	7	1.00	15.4	0.24 (3)	5.5	–
1441−6137	14:41:44.3 (1)	−61:37:24 (2)	315.65	−1.50	6	1.10	15.9	0.15 (3)	18.0	–
1449−5846	14:49:25.43 (6)	−58:46:40.4 (7)	317.72	+0.66	8	1.07	14.2	0.28 (4)	15.0	27
1452−6036	14:52:51.898 (8)	−60:36:31.35 (6)	317.30	−1.17	3	0.25	100.0	1.40 (15)	4.2	18
1457−5900	14:57:39.0 (2)	−59:00:51 (3)	318.56	−0.03	3	0.95	16.6	0.24 (3)	62	–
1457−5902	14:57:31.9 (1)	−59:02:04 (2)	318.54	−0.04	2	0.85	30.8	0.26 (4)	8.4	–
1501−5637	15:01:51.0 (4)	−56:37:48 (5)	320.18	+1.81	13	0.09	16.4	0.21 (3)	25	–
1502−5828	15:02:43.8 (3)	−58:28:42 (6)	319.39	+0.13	10	0.98	20.7	0.50 (6)	22	–
1502−6128	15:02:29.84 (5)	−61:28:50.3 (5)	317.92	−2.48	3	1.18	24.0	0.56 (7)	29	53
1504−5621	15:04:49.14 (7)	−56:21:32 (1)	320.67	+1.85	6	0.40	25.9	0.24 (3)	11.0	–
1509−5850	15:09:27.13 (3)	−58:50:56.1 (5)	319.97	−0.62	7	0.13	12.3	0.15 (3)	4.7	–
1509−6015	15:09:07.5 (1)	−60:15:18.6 (6)	319.23	−1.81	1	0.46	13.6	0.17 (3)	13.0	–
1511−5414	15:11:51.308 (6)	−54:14:40.3 (1)	322.60	+3.18	3	0.86	86.7	0.75 (8)	5.9	11
1511−5835	15:11:07.0 (3)	−58:35:28 (1)	320.29	−0.51	1	1.04	25.2	0.50 (6)	16.0	–
1512−5431	15:12:05.7 (2)	−54:31:19 (3)	322.49	+2.92	4	0.99	24.9	0.38 (5)	110	–
1514−5925	15:14:59.10 (4)	−59:25:43.3 (5)	320.28	−1.48	13	0.58	14.5	0.27 (4)	4.8	–
1515−5720	15:15:09.3 (1)	−57:20:49 (3)	321.39	+0.28	7	0.81	12.5	0.20 (3)	31	–
1522−5525	15:22:06.7 (1)	−55:25:17.5 (9)	323.23	+1.40	12	0.44	29.3	0.25 (4)	10.0	–
1524−5625	15:24:49.86 (4)	−56:25:23.4 (6)	323.00	+0.35	3	1.10	27.0	0.83 (9)	12.0	–
1524−5706	15:24:21.43 (7)	−57:06:35 (2)	322.57	−0.19	13	0.51	37.1	0.41 (5)	22	43
1525−5417	15:25:28.35 (6)	−54:17:20 (1)	324.26	+2.08	9	0.38	24.8	0.18 (3)	15.0	–
1525−5605	15:25:41.45 (9)	−56:05:13 (2)	323.29	+0.56	3	0.59	17.3	0.25 (4)	25	–
1526−5633	15:26:41.2 (1)	−56:33:43 (3)	323.14	+0.09	1	0.77	9.9	0.11 (2)	13.0	–
1529−5355	15:29:57.6 (3)	−53:55:36 (5)	325.01	+2.01	8	0.36	25.1	0.37 (5)	56	–
1529−5611	15:29:35.8 (6)	−56:11:29 (13)	323.68	+0.17	4	0.54	14.2	0.14 (2)	42	–
1531−5610	15:31:27.91 (1)	−56:10:55.0 (1)	323.90	+0.03	4	0.49	43.9	0.60 (7)	5.8	11
1532−5308	15:32:35.5 (1)	−53:08:06 (2)	325.78	+2.43	1	0.69	22.5	0.25 (4)	26	–
1535−5450	15:35:58.26 (6)	−54:50:26 (1)	325.19	+0.76	10	0.67	14.7	0.17 (3)	9.4	–
1535−5848	15:35:16.76 (4)	−58:48:27.7 (3)	322.80	−2.41	3	0.93	21.6	0.35 (4)	5.8	12
1537−5153	15:37:15.73 (6)	−51:53:06 (1)	327.09	+3.04	10	0.92	12.7	0.07 (2)	23	–
1538−5638	15:38:05.7 (2)	−56:38:12 (4)	324.38	−0.87	10	1.16	14.0	0.28 (4)	46	–
1538−5750	15:38:08.41 (4)	−57:50:17.1 (6)	323.72	−1.83	6	0.07	13.4	0.06 (2)	4.7	145
1539−5521	15:39:07.97 (7)	−55:21:11.2 (8)	325.26	+0.08	2	0.57	8.9	0.14 (2)	23	–
1541−5535	15:41:49.6 (4)	−55:35:01 (5)	325.42	−0.34	3	0.78	16.2	0.22 (3)	14.0	–
1542−5303	15:42:54.51 (4)	−53:03:41 (1)	327.07	+1.58	7	0.25	36.2	0.35 (4)	54	72
1543−5013	15:43:58.25 (8)	−50:13:58 (1)	328.93	+3.72	11	0.78	11.3	0.17 (3)	15.0	–
1546−5302	15:46:07.4 (1)	−53:02:23.0 (9)	327.47	+1.30	9	0.90	29.0	0.32 (4)	8.8	190
1547−5839	15:47:34.99 (4)	−58:39:09.8 (7)	324.17	−3.24	1	0.89	18.6	0.41 (5)	13.0	42
1548−4821	15:48:23.26 (3)	−48:21:49.7 (6)	330.65	+4.75	2	0.88	18.1	0.51 (6)	12.0	–
1548−4927	15:48:19.47 (3)	−49:27:40.4 (5)	329.96	+3.90	10	0.50	90.3	0.69 (8)	12.0	20
1549−5722	15:49:47.9 (1)	−57:22:02 (1)	325.20	−2.42	5	0.27	13.7	0.10 (2)	13.0	–
1550−5242	15:50:02.95 (5)	−52:42:07.0 (8)	328.14	+1.20	13	0.77	28.0	0.32 (4)	11.0	22
1550−5317	15:50:04.8 (1)	−53:17:21 (2)	327.78	+0.74	1	1.42	9.7	0.40 (5)	85	–
1554−5512	15:54:40.5 (4)	−55:12:33 (12)	327.09	−1.17	12	0.62	10.7	0.11 (2)	63	–
1556−5358	15:56:51.5 (3)	−53:58:55 (2)	328.12	−0.44	9	0.95	33.8	0.53 (6)	29	–

Table 1 – *continued*

PSR J	RA (J2000) (h m s)	Dec. (J2000) (° ′ ″)	l (deg)	b (deg)	Beam	Radial dist.	S/N ratio	S_{1400} (mJy)	W_{50} (ms)	W_{10} (ms)
1602−4957	16:02:18.2 (1)	−49:57:32 (4)	331.37	+2.07	7	0.87	10.3	0.17 (3)	29	–
1610−5303	16:10:12.82 (9)	−53:03:49 (3)	330.21	−1.06	10	0.82	37.5	0.76 (9)	44	–
1611−4811	16:11:02.7 (4)	−48:11:39 (6)	333.62	+2.42	10	0.26	9.9	0.08 (2)	33	–
1612−5136	16:12:00.6 (3)	−51:36:54 (6)	331.40	−0.19	4	0.31	12.9	0.20 (3)	125	–
1614−5144	16:14:45.7 (5)	−51:44:49 (9)	331.62	−0.58	4	0.66	10.7	0.16 (3)	68	–
1614−5402	16:14:50.38 (6)	−54:02:47 (2)	330.04	−2.25	9	0.57	22.5	0.25 (4)	14.0	–
1615−5444	16:15:01.191 (8)	−54:44:32.4 (2)	329.58	−2.77	8	0.54	62.5	0.59 (7)	6.5	20
1618−4723	16:18:06.80 (1)	−47:23:19.1 (3)	335.04	+2.18	3	1.12	36.7	1.00 (11)	11.0	16
1621−5243	16:21:55.8 (1)	−52:43:44 (3)	331.72	−2.04	5	0.58	19.5	0.27 (4)	17.0	–
1624−4721	16:24:54.89 (8)	−47:21:27 (2)	335.87	+1.39	7	0.39	11.6	0.15 (3)	18.0	–
1626−4537	16:26:48.98 (1)	−45:37:25.6 (5)	337.35	+2.37	2	0.47	83.7	1.10 (12)	12.0	24
1627−5547	16:27:21.08 (2)	−55:47:52.4 (4)	330.07	−4.76	2	1.14	25.6	0.65 (7)	14.0	27
1628−4828	16:28:30.9 (4)	−48:28:42 (9)	335.49	+0.18	1	0.94	13.1	0.29 (4)	240	–
1630−4719	16:30:02.47 (5)	−47:19:42 (2)	336.50	+0.79	1	0.64	49.1	0.46 (6)	10.0	19
1633−4805	16:33:05.4 (1)	−48:05:36 (4)	336.29	−0.11	7	0.79	13.9	0.23 (3)	48	–
1635−4513	16:35:55.4 (3)	−45:13:27 (17)	338.73	+1.47	10	0.50	16.4	0.25 (4)	75	–
1635−4944	16:35:55.4 (1)	−49:44:36 (2)	335.39	−1.57	6	0.87	19.6	0.40 (5)	40	–
1636−4803	16:36:32.0 (2)	−48:03:55 (9)	336.70	−0.51	7	1.15	43.7	1.10 (12)	44	–
1636−4933	16:36:55.15 (5)	−49:33:10 (3)	335.64	−1.56	1	0.93	24.0	0.45 (6)	17.0	–
1637−4335	16:37:56.8 (1)	−43:35:42 (5)	340.18	+2.30	9	0.75	8.7	0.18 (3)	40	–
1637−4642	16:37:13.77 (8)	−46:42:15 (1)	337.79	+0.31	7	0.72	29.5	0.78 (9)	17.0	–
1637−4721	16:37:11.4 (1)	−47:21:03 (8)	337.30	−0.12	4	0.75	24.1	0.42 (5)	21	–
1638−4344	16:38:52.88 (5)	−43:44:04 (1)	340.19	+2.08	9	0.57	12.1	0.17 (3)	34	–
1638−4608	16:38:22.98 (1)	−46:08:11.6 (5)	338.34	+0.54	5	0.85	19.5	0.33 (4)	7.7	–
1638−5226	16:38:59.96 (3)	−52:26:57.4 (4)	333.70	−3.74	4	1.12	16.9	0.60 (7)	13.0	–
1639−4359	16:39:06.85 (4)	−43:59:52 (2)	340.02	+1.87	11	0.78	69.7	0.92 (10)	24	35
1640−4648	16:40:47.62 (6)	−46:48:45 (2)	338.11	−0.22	3	0.62	10.8	0.26 (4)	15.0	–
1640−4951	16:40:43.56 (3)	−49:51:02.1 (7)	335.83	−2.22	11	0.38	18.0	0.15 (3)	13.0	–
1643−4522	16:43:20.40 (7)	−45:22:01 (2)	339.49	+0.41	11	0.35	12.2	0.11 (2)	21	–
1643−4550	16:43:13.52 (2)	−45:50:54.5 (5)	339.12	+0.10	8	0.75	16.9	0.34 (4)	15.0	27
1646−4308	16:46:55.3 (2)	−43:08:07 (4)	341.60	+1.37	12	0.98	11.5	0.33 (4)	185	–
1648−4458	16:48:13.0 (1)	−44:58:26 (3)	340.35	+0.01	10	0.73	19.7	0.55 (7)	42	–
1648−4611	16:48:22.02 (3)	−46:11:16 (1)	339.44	−0.79	8	0.05	21.5	0.58 (7)	12.0	–
1649−4653	16:49:24.5 (1)	−46:53:09 (6)	339.02	−1.38	10	0.80	16.0	0.31 (4)	18.0	–
1650−4126	16:50:13.174 (5)	−41:26:33.8 (3)	343.29	+2.00	13	1.02	14.8	0.29 (4)	7.6	15
1650−4341	16:50:44.68 (1)	−43:41:30.8 (5)	341.62	+0.48	2	0.64	14.8	0.26 (4)	20	–
1651−4519	16:51:57.2 (5)	−45:19:11 (8)	340.51	−0.72	3	1.06	18.5	0.54 (6)	52	–
1653−4315	16:53:29.7 (2)	−43:15:01 (5)	342.28	+0.38	10	0.39	21.8	0.53 (6)	105	–
1653−4854	16:53:56.7 (1)	−48:54:51 (4)	337.94	−3.26	3	1.06	9.8	0.18 (3)	75	–
1654−4140	16:54:23.5 (1)	−41:40:24 (3)	343.61	+1.25	8	0.25	48.2	0.71 (8)	19.0	–
1657−4432	16:57:36.73 (4)	−44:32:20 (1)	341.74	−1.01	3	0.58	27.0	0.38 (5)	13.0	30
1658−4306	16:58:16.6 (3)	−43:06:50 (7)	342.93	−0.21	1	1.31	26.9	0.80 (9)	97	–
1659−4316	16:59:56.38 (4)	−43:16:06 (2)	343.00	−0.55	5	0.99	13.3	0.21 (3)	11.0	–
1659−4439	16:59:39.44 (4)	−44:39:01 (1)	341.88	−1.36	1	0.57	30.7	0.42 (5)	18.0	–
1700−4939	17:00:22.56 (4)	−49:39:15 (1)	338.01	−4.54	13	0.66	15.1	0.17 (3)	13.0	79
1702−3932	17:02:14.36 (3)	−39:32:40 (2)	346.20	+1.40	12	0.96	15.8	0.30 (4)	14.0	–
1702−4128	17:02:52.52 (1)	−41:28:48.2 (5)	344.74	+0.12	8	1.01	34.7	1.10 (12)	15.0	43
1702−4310	17:02:26.94 (5)	−43:10:40 (2)	343.35	−0.85	6	0.82	37.9	0.72 (8)	16.0	–
1702−4428	17:02:52.6 (4)	−44:28:03 (7)	342.38	−1.70	4	1.07	18.6	0.38 (5)	74	–
1703−4442	17:03:20.59 (3)	−44:42:42 (1)	342.23	−1.92	6	1.07	16.9	0.21 (3)	12.0	58
1705−3936	17:05:37.1 (3)	−39:36:29 (6)	346.55	+0.85	9	0.46	15.4	0.33 (4)	22	–
1705−3950	17:05:29.84 (3)	−39:50:59 (1)	346.34	+0.72	5	1.00	52.6	1.50 (16)	8.2	34
1705−4108	17:05:20.4 (1)	−41:08:44 (8)	345.29	−0.04	8	0.25	46.6	1.30 (14)	44	–
1706−3839	17:06:21.3 (2)	−38:39:51 (13)	347.39	+1.30	5	0.89	12.7	0.20 (3)	26	–
1706−4310	17:06:04.51 (5)	−43:10:21 (3)	343.76	−1.37	4	0.37	18.4	0.28 (4)	16.0	–
1707−4341	17:07:40.11 (1)	−43:41:12.0 (6)	343.52	−1.91	1	0.82	39.6	0.46 (6)	12.0	29
1707−4729	17:07:15.547 (7)	−47:29:34.5 (3)	340.42	−4.14	12	1.31	33.5	1.9 (2)	6.3	37
1708−3827	17:08:16.5 (6)	−38:27:36 (15)	347.78	+1.12	13	1.18	14.9	0.42 (5)	40	–

Table 1 – *continued*

PSR J	RA (J2000) (h m s)	Dec. (J2000) (° ′ ″)	l (deg)	b (deg)	Beam	Radial dist.	S/N ratio	S_{1400} (mJy)	W_{50} (ms)	W_{10} (ms)
1709−3626	17:09:45.15 (2)	−36:26:03.6 (9)	349.58	+2.10	7	1.11	29.8	0.58 (7)	17.0	31
1709−4342	17:09:30.9 (4)	−43:42:14 (13)	343.71	−2.19	6	0.82	9.7	0.14 (2)	50	–
1710−4148	17:10:23.75 (4)	−41:48:19 (2)	345.33	−1.20	12	0.26	16.2	0.31 (4)	12.0	–
1711−3826	17:11:44.45 (9)	−38:26:14 (5)	348.20	+0.59	10	0.51	11.7	0.16 (3)	24	–
1713−3844	17:13:02.3 (1)	−38:44:29 (9)	348.10	+0.21	4	0.84	18.9	0.26 (4)	17.0	–
1715−3903	17:15:14.3 (1)	−39:03:02 (3)	348.10	−0.32	10	1.07	21.6	0.46 (6)	8.5	–
1715−4034	17:15:40.99 (8)	−40:34:22 (4)	346.91	−1.28	5	0.68	105.5	1.60 (17)	83	–
1717−3737	17:17:15.96 (2)	−37:37:36 (1)	349.49	+0.18	4	0.89	26.8	0.69 (8)	22	51
1717−3847	17:17:18.4 (5)	−38:47:03 (20)	348.55	−0.49	4	0.00	23.0	0.30 (4)	287	–
1717−4043	17:17:47.91 (6)	−40:43:50 (2)	347.02	−1.69	11	0.64	25.7	0.54 (6)	41	–
1717−40433	17:17:02.0 (4)	−40:43:31 (9)	346.94	−1.57	11	0.58	24.2	0.41 (5)	38	–
1719−4302	17:19:48.77 (1)	−43:02:11.4 (6)	345.34	−3.32	13	0.52	27.1	0.37 (5)	5.7	11
1725−3848	17:25:00.1 (5)	−38:48:36 (14)	349.38	−1.74	1	0.68	14.4	0.140 (20)	32	–
1725−4043	17:25:41.42 (4)	−40:43:11 (2)	347.87	−2.92	7	1.24	14.9	0.34 (4)	50	99
1732−3729	17:32:20.81 (5)	−37:29:05 (3)	351.29	−2.21	1	0.36	38.8	0.31 (4)	40	73
1736−3511	17:36:02.7 (3)	−35:11:56 (11)	353.61	−1.60	2	0.63	14.2	0.18 (3)	15.0	–
1751−3323	17:51:32.75 (1)	−33:23:39 (2)	356.83	−3.38	13	0.32	79.8	1.30 (14)	8.4	32
1829−0734[J]	18:29:05.37 (4)	−07:34:22 (3)	23.65	+1.48	2	0.78	25.2	0.45 (6)	7.1	–
1834−1710[J]	18:34:53.401 (6)	−17:10:50 (2)	15.77	−4.21	4	0.49	40.3	1.00 (11)	14.0	21
1842−0905[J]	18:42:22.138 (7)	−09:05:24.6 (8)	23.81	−2.14	8	0.94	22.6	0.81 (9)	7.7	22
1845−0743[J]	18:45:57.18 (1)	−07:43:38.4 (6)	25.43	−2.30	2	1.08	106.3	2.7 (3)	4.7	11
1853+0545[J]	18:53:58.418 (5)	+05:45:55.2 (3)	38.35	+2.06	4	0.91	64.6	1.60 (17)	9.5	–
1857+0526[J]	18:57:15.856 (8)	+05:26:28.7 (5)	38.44	+1.19	4	0.54	39.9	0.66 (8)	9.7	26
1904+0800[J]	19:04:03.50 (2)	+08:00:52.6 (9)	41.50	+0.86	9	0.79	20.6	0.36 (5)	9.2	–
1913+0446[J]	19:13:50.82 (4)	+04:46:06 (2)	39.74	−2.79	2	1.33	37.2	0.48 (6)	16.0	60

(Camilo et al. 2001a; D'Amico et al. 2001; Torres, Butt & Camilo 2001). Here we comment on further possible pulsar γ-rays counterparts and discuss how many of the positional coincidences may be genuine rather than due to chance alignments.

In Table 4 we list all pulsar/EGRET point source positional associations, where the pulsar position deviates from the nominal EGRET source position by less than the 95 per cent error box radius, i.e. $\Delta\Phi/\theta_{95} \leqslant 1$, where $\Delta\Phi$ is the difference in the two positions. We list *all* EGRET point sources including those already identified as pulsars (ID = P), galaxies (ID = G) and active galactic nuclei (ID = A). As a result of the large number of newly discovered pulsars in the Galactic plane, often several pulsars lie in the same error box. For EGRET sources that have not been identified previously (ID = ?), we can attempt to judge the likelihood of the individual possible associations by comparing the properties of the γ-ray source and the corresponding pulsar(s).

For the EGRET sources, we summarize their characteristics as listed in the 3EG catalogue (Hartman et al. 1999). Besides the error box size, θ_{95}, we list a computed γ-ray flux, $\bar{F}$ ($E > 100$ MeV). We have used the flux values as derived by Hartman et al. in units of 10^{-8} photon s^{-1} cm^{-2}, assuming a spectral index of 2.0, to derive values in units of erg s^{-1} cm^{-2}, where we followed the calculations by D'Amico et al. (2001).

It has been shown for the known genuine pulsar/EGRET source associations that pulsars are steady γ-ray sources (e.g. McLaughlin et al. 1996). Therefore, we also quote for all EGRET sources in Table 4 a variability index, V, as defined by McLaughlin et al. (1996). Values for V are taken from an updated list presented by McLaughlin (2001) and are typically found to be <1 for pulsars.

For each EGRET source we list the possible pulsar counterpart(s). Pulsar/EGRET source pairs that have been proposed in the literature previously are listed with corresponding references. Plausible associations involving pulsars discovered in the PMPS are discussed in more detail later. All such multibeam pulsars have been published separately, in this work, or in Papers I or II. A few newly discovered pulsars listed here will soon be presented with all parameters in a forthcoming paper (Paper IV, in preparation).

In order to assess the likelihood of an association to be genuine, one has to compare the γ-ray luminosity, L_γ, to the spin-down luminosity, $\dot{E}$, of the pulsar. Typically, this efficiency, $\eta \equiv L_\gamma/\dot{E}$, is assumed to lie in a range from 0.01 to about 20 per cent (e.g. Torres et al. 2001). Deriving these numbers requires conversion of the γ-ray flux measured by EGRET, $\bar{F}$, into the luminosity, L_γ. This is a non-trivial task, however, as the beaming fraction, f, for the high-energy emission is unknown. One typically assumes a beaming fraction of 1 sr, i.e. $f = 1/4\pi$ (cf. Torres et al. 2001).

In order to derive the γ-ray luminosity, one must also use a distance estimate, which is usually based on the dispersion measure. As some pulsar distances derived from the dispersion measure differ significantly when applying the new NE2001 electron density model rather than the previously used TC93 model, we quote distances derived from both models for comparison. For instance, the distance for PSR J0218+4232 is reduced from 5.9 kpc (TC93) to only 2.9 kpc (NE2001), making it a more average γ-ray pulsar in terms of $\dot{E}/d^2$ and efficiency, although it remains the only millisecond pulsar detected at γ-ray energies. Similarly, for PSR B1055−52 the new NE2001 distance estimate is much smaller than the TC93 one, resulting in a decrease of the efficiency from 18.4 to 4.1 per cent. This dramatic change has important implications for the discussions of genuine EGRET source/pulsar pairs as it was basically PSR B1055−52 that in the past had set the upper limit for the efficiency range assumed to be possible, i.e. $\eta \leqslant 20$ per cent. The much reduced value for this pulsar may now imply that real associations should also accommodate much lower values for η. In

Table 2. Periods, period derivatives and dispersion measures for 200 pulsars discovered in the Parkes Multibeam Pulsar Survey. We also give the MJD of the epoch used for period determination, the number of TOAs included and the MJD range covered, as well as the rms of the post-fit timing residuals. Asterisks indicate those pulsars which exhibit significant timing noise that has been removed, to first order, by the fitting of a period second derivative.

PSR J	Period, P (s)	$\dot{P}$ (10^{-15})	Epoch (MJD)	$N_{\rm toa}$	Data span (MJD)	Residual (ms)	DM ($\rm cm^{-3}$ pc)
0831−4406	0.311 673 518 473 (11)	1.279 (6)	51396	38	51215–51577	0.47	254.0 (5)
0834−4159	0.121 116 349 354 (15)	4.437 (8)	51505	27	51299–51710	1.88	240.5 (15)
0855−4644	0.064 685 817 073 (3)	7.2626 (13)	51368	71	51158–52249	0.90	238.2 (16)
0855−4658	0.575 072 382 58 (4)	13.625 (20)	51395	39	51158–51577	1.17	472.7 (12)
0945−4833	0.331 585 598 7755 (18)	4.8291 (6)	51703	35	51464–51940	0.15	98.1 (3)
1000−5149	0.255 677 098 4252 (20)	0.9595 (6)	51368	35	51158–51577	0.15	72.8 (3)
1012−5830	2.133 591 2144 (3)	37.65 (6)	51702	31	51462–51940	2.54	294 (4)
1013−5934	0.442 900 630 729 (4)	0.5579 (20)	51397	28	51215–51577	0.10	379.78 (17)
1015−5719	0.139 881 677 595 (4)	57.3680 (12)	51476	48	51260–51692	0.65	278.7 (6)
1019−5749	0.162 498 709 997 (8)	20.077 (3)	51371	42	51158–51582	0.98	1039.4 (11)
1020−5921	1.238 305 344 23 (11)	40.47 (8)	51397	25	51215–51578	1.26	80 (3)
1022−5813	1.643 726 0020 (5)	145.4 (3)	51398	24	51158–51577	3.04	714 (8)
1031−6117	0.306 410 837 119 (10)	1.784 (5)	51496	35	51299–51692	0.77	506.8 (12)
1035−6345	0.579 576 736 318 (6)	0.3504 (12)	51875	25	51632–52118	0.62	189.7 (9)
1043−6116	0.288 601 695 277 (5)	10.404 (3)	51368	36	51158–51577	0.39	449.2 (4)
1052−5954	0.180 591 500 693 (10)	19.9831 (17)	51683	38	51411–51955	1.71	491 (3)
1054−5943	0.346 908 957 903 (13)	4.074 (8)	51395	25	51211–51577	0.51	330.7 (6)
1055−6236	0.448 635 442 46 (3)	0.708 (7)	51703	26	51464–51940	1.14	149.7 (15)
1058−5957	0.616 270 272 343 (16)	0.657 (4)	51446	24	51213–51678	0.39	334.0 (11)
1103−6025	0.396 586 748 928 (5)	0.9904 (19)	51489	22	51299–51678	0.16	275.9 (3)
1107−6143	1.799 395 6675 (4)	155.77 (20)	51397	29	51215–51577	2.48	406 (3)
1117−6154	0.505 097 149 18 (5)	12.51 (3)	51397	24	51216–51577	1.06	493.6 (9)
1117−6447	1.155 271 9604 (3)	0.24 (7)	51703	29	51464–51940	5.59	303 (6)
1124−5638	0.185 559 973 402 (11)	0.009 (5)	51752	21	51562–51940	0.69	289.5 (16)
1124−6421	0.479 098 584 52 (7)	0.62 (3)	51400	26	51216–51582	1.51	298 (3)
1128−6219	0.515 983 510 50 (11)	0.011 (5)	51660	62	51085–51753	8.62	675 (9)
1130−5826	0.162 323 475 501 (3)	0.01589 (19)	51696	28	51158–52233	0.57	261.1 (7)
1132−5627	0.175 166 247 082 (10)	0.068 (4)	52165	24	51984–52345	0.49	305.7 (8)
1141−6545[B]	0.393 897 833 9002 (22)	4.3070 (2)	51370	30	51369–51562	0.06	116.03 (8)
1148−6415	3.241 028 5031 (8)	2.7 (4)	51474	22	51260–51691	4.52	241.0 (6)
1152−6012	0.376 569 565 76 (5)	6.685 (19)	51397	19	51216–51577	0.99	74 (3)
1154−6250	0.282 011 710 65 (3)	0.559 (5)	51464	38	51217–51710	1.95	74 (6)
1159−6409	0.667 485 533 54 (6)	0.024 (4)	51767	16	51300–51806	2.05	178 (5)
1201−6306	0.592 136 029 08 (5)	3.555 (11)	51676	25	51411–51940	2.03	683 (3)
1211−6324	0.433 083 926 199 (17)	0.257 (8)	51489	20	51300–51678	0.56	333.8 (11)
1214−5830	0.909 822 701 18 (4)	0.0534 (15)	51546	29	51411–52115	0.45	141.1 (7)
1222−5738	1.081 163 5266 (13)	0.15 (5)	51587	18	51682–52115	1.98	74 (6)
1225−6035	0.626 323 941 978 (18)	0.288 (8)	51752	20	51562–51940	0.37	176.1 (10)
1231−6303	1.351 236 2992 (6)	1.4 (25)	51397	21	51216–51577	4.51	301 (10)
1233−6312	0.564 759 3892 (4)	6.92 (16)	51396	18	51214–51577	6.31	414 (13)
1233−6344	0.756 891 933 63 (7)	3.878 (18)	51451	28	51214–51688	2.43	495 (9)
1235−6354	0.256 777 653 406 (12)	0.197 (4)	51700	26	51458–51940	1.07	439.9 (19)
1237−6725	2.110 974 117 94 (14)	2.19 (4)	51702	22	51462–51940	1.36	179 (3)
1243−5735	0.471 224 877 69 (16)	0.080 (7)	51590	20	51632–52115	1.08	270.6 (19)
1248−6344	0.198 335 136 357 (8)	16.918 (20)	51451	40	51214–51691	1.16	433.3 (15)
1249−6507	0.434 444 873 08 (3)	0.0121 (14)	51724	17	51214–51577	1.40	215 (4)
1254−6150	0.184 502 203 069 (7)	0.624 (3)	51368	23	51158–51577	0.64	95 (3)
1255−6131	0.657 973 630 34 (3)	4.000 (7)	51449	27	51217–51680	0.72	206.5 (17)
1301−6310*	0.663 829 647 70 (4)	56.433 (5)	51487	24	51221–51753	0.99	86.1 (12)
1302−6313	0.967 846 2129 (4)	6.33 (8)	51342	12	51100–51582	5.44	500 (21)
1306−6242	0.981 902 118 48 (9)	5.86 (3)	51448	25	51214–51680	2.21	480 (6)
1309−6526	0.398 292 162 785 (20)	0.0184 (15)	51767	32	51300–51958	1.67	340 (4)
1314−6101	2.948 389 6038 (15)	11.7 (9)	51396	22	51213–51577	7.05	309 (13)
1319−6105	0.421 118 114 249 (6)	1.5012 (11)	51709	27	51458–51958	0.28	442.2 (5)
1322−6329	2.764 209 4208 (5)	11.08 (10)	51456	22	51220–51691	2.80	659 (9)
1324−6146	0.844 108 5753 (3)	5.58 (14)	51397	27	51214–51578	4.54	828 (9)
1324−6302	2.483 803 693 00 (10)	0.979 (9)	51523	21	51087–51958	1.16	497 (5)

Table 2 – *continued*

PSR J	Period, P (s)	$\dot{P}$ (10^{-15})	Epoch (MJD)	$N_{\rm toa}$	Data span (MJD)	Residual (ms)	DM ($\rm cm^{-3}$ pc)
1329−6158	1.565 217 9638 (8)	33.9 (3)	51490	21	51301–51678	5.85	514 (11)
1339−6618	0.558 179 221 85 (5)	0.35 (3)	51760	19	51562–51958	1.43	241 (3)
1344−6059	0.540 102 321 40 (6)	0.043 (4)	51676	23	51099–52252	5.25	435 (7)
1354−6249	2.951 938 334 (3)	14.8 (11)	51396	14	51214–51577	7.67	254 (17)
1355−5925	1.213 381 226 74 (5)	5.986 (11)	51730	22	51501–51958	0.63	354.8 (9)
1355−6206	0.276 603 043 150 (10)	0.0031 (6)	51724	25	51214–51691	1.28	547 (3)
1403−6310	0.399 170 176 93 (5)	0.094 (20)	51341	17	51158–51522	1.00	305 (3)
1406−5806	0.288 349 244 25 (5)	0.611 (10)	51730	25	51501–51958	2.93	229 (3)
1413−6141	0.285 624 620 18 (16)	333.44 (15)	51500	23	50849–51294	5.07	677 (8)
1418−5945	1.672 595 6812 (3)	0.271 (17)	51668	13	51101–51471	3.83	369 (15)
1420−6048	0.068 179 876 59 (2)	83.167 (3)	51600	25	51212–51782	3.33	360.0 (3)
1424−5822	0.366 734 060 217 (6)	3.943 (3)	51368	17	51158–51577	0.23	323.9 (6)
1424−6438	1.023 503 699 13 (9)	0.24 (7)	51780	17	51602–51956	3.39	248 (5)
1425−5723	0.353 262 920 24 (8)	0.022 (20)	51468	25	51632–52114	0.62	43.4 (13)
1425−5759	0.707 867 605 76 (4)	0.742 (16)	51496	20	51301–51691	0.79	325 (5)
1434−6006	0.306 367 862 68 (4)	3.020 (17)	51396	17	51214–51577	1.21	332 (4)
1441−6137	1.175 840 022 90 (10)	0.36 (5)	51670	24	51459–51880	1.80	166 (3)
1449−5846	0.463 329 577 191 (18)	0.086 (9)	51507	22	51302–51710	0.66	216.6 (18)
1452−6036	0.154 991 357 9183 (8)	1.44989 (10)	51630	38	51302–51956	0.20	349.7 (3)
1457−5900	1.498 637 4368 (4)	3.66 (7)	51462	21	51213–51710	3.50	175 (4)
1457−5902	0.390 739 364 18 (5)	12.306 (14)	51312	18	51100–51523	1.24	477.2 (19)
1501−5637	0.782 948 5661 (3)	0.17 (8)	51506	18	51299–51711	4.36	258 (10)
1502−5828	0.668 105 150 91 (14)	36.40 (8)	51297	20	51101–51491	2.55	584 (4)
1502−6128	0.842 103 840 00 (3)	1.348 (7)	51708	25	51460–51956	0.90	256.5 (14)
1504−5621	0.412 985 199 81 (3)	5.529 (12)	51505	18	51299–51710	1.10	143 (5)
1509−5850	0.088 921 760 489 (3)	9.1698 (7)	51463	36	51214–51710	0.87	137.7 (9)
1509−6015	0.339 038 448 70 (4)	2.121 (12)	51759	19	51562–51956	1.01	423.6 (17)
1511−5414	0.200 383 695 9221 (17)	0.4848 (3)	51684	25	51411–51956	0.18	84.76 (17)
1511−5835	0.301 510 550 02 (4)	0.344 (19)	51397	22	51214–51578	1.61	332 (3)
1512−5431	2.040 531 5742 (3)	1.92 (6)	51709	23	51460–51957	3.40	219 (6)
1514−5925	0.148 796 488 226 (5)	2.8829 (7)	51487	26	51220–51753	0.74	194.1 (13)
1515−5720	0.286 646 196 50 (4)	6.098 (8)	51478	18	51244–51711	1.90	482 (5)
1522−5525	1.389 604 6876 (16)	3.30 (8)	51097	20	51214–51578	1.02	79 (3)
1524−5625	0.078 218 548 881 (5)	38.95005 (19)	51733	56	51214–52252	1.73	152.7 (10)
1524−5706	1.116 048 619 27 (8)	356.47 (5)	51297	21	51101–51491	1.24	833 (3)
1525−5417	1.011 694 217 72 (7)	16.174 (14)	51463	30	51214–51710	1.86	235 (3)
1525−5605	0.280 348 662 06 (4)	0.116 (7)	51467	32	51220–51712	2.62	338 (3)
1526−5633	0.301 887 896 63 (5)	0.123 (17)	51490	20	51299–51680	1.71	329 (4)
1529−5355	0.891 264 5399 (4)	0.81 (4)	51485	24	51215–51753	6.25	292 (9)
1529−5611	0.822 248 7311 (5)	4.1 (3)	51311	16	51099–51523	8.04	149 (10)
1531−5610	0.084 201 682 8855 (8)	13.7406 (3)	51448	31	51215–51680	0.23	110.9 (4)
1532−5308	0.443 824 608 30 (4)	0.065 (6)	51587	29	51215–51957	3.67	181 (3)
1535−5450	0.566 734 156 72 (4)	14.338 (10)	51448	17	51215–51680	1.23	219.8 (14)
1535−5848	0.307 177 662 775 (7)	2.716 (3)	51760	20	51562–51957	0.34	107.0 (7)
1537−5153	1.528 124 105 66 (12)	4.172 (12)	51423	31	51092–51753	2.15	93 (4)
1538−5638	0.843 980 396 88 (14)	7.12 (8)	51490	19	51299–51680	2.53	546 (7)
1538−5750	0.506 5677 (10)	0.042 (3)	51032	34	51213–51753	1.05	91 (4)
1539−5521	1.004 958 318 13 (8)	0.728 (8)	51730	27	51300–51957	1.66	380 (5)
1541−5535	0.295 837 553 45 (9)	75.02 (3)	51527	25	51300–51753	5.70	428 (5)
1542−5303	1.207 567 765 26 (6)	77.80 (3)	51491	17	51300–51680	0.57	265.7 (12)
1543−5013	0.644 255 0645 (6)	10.132 (17)	51456	22	51681–52117	1.40	211 (3)
1546−5302	0.580 839 886 15 (4)	11.80 (3)	51398	22	51215–51580	1.11	287 (3)
1547−5839	0.242 190 323 768 (10)	0.594 (3)	51876	32	51634–52117	1.22	222.3 (12)
1548−4821	0.145 654 719 47 (3)	0.0008 (11)	51587	25	51686–52117	0.47	126.0 (5)
1548−4927	0.602 738 077 704 (19)	4.047 (3)	51685	25	51411–51958	0.76	141.2 (6)
1549−5722	0.497 772 394 00 (8)	0.047 (10)	51685	21	51411–51959	2.55	102 (4)
1550−5242	0.749 658 949 57 (4)	17.774 (6)	51335	20	51089–51580	0.75	337.7 (18)
1550−5317	1.421 124 345 44 (13)	0.935 (11)	51535	32	51099–51969	3.95	600 (8)

Table 2 – *continued*

PSR J	Period, P (s)	$\dot{P}$ (10^{-15})	Epoch (MJD)	$N_{\rm toa}$	Data span (MJD)	Residual (ms)	DM ($\rm cm^{-3}$ pc)
1554−5512	3.418 039 313 (3)	31.2 (10)	51491	14	51302–51678	5.99	450 (12)
1556−5358	0.994 680 686 73 (14)	10.42 (8)	51398	21	51215–51580	2.21	436 (3)
1602−4957	0.819 990 036 85 (14)	15.94 (3)	51487	17	51220–51753	2.82	319 (4)
1610−5303	0.786 468 023 52 (9)	2.615 (12)	51488	27	51221–51753	2.48	380.1 (8)
1611−4811	1.296 850 239 (3)	1.95 (14)	51687	15	51717–52115	2.83	221 (8)
1612−5136	0.483 310 511 32 (12)	3.784 (12)	51348	44	50939–51755	11.56	1173 (12)
1614−5144	1.534 008 1422 (5)	7.44 (5)	51281	17	50849–51371	8.28	748 (13)
1614−5402	0.572 592 271 92 (6)	0.029 (8)	51482	18	51221–51741	1.54	300 (4)
1615−5444	0.360 957 675 308 (4)	0.3377 (7)	51482	24	51221–51741	0.22	312.6 (5)
1618−4723	0.203 552 877 86 (5)	1.9926 (8)	51097	25	51686–52116	0.21	134.7 (3)
1621−5243	0.371 924 138 84 (6)	0.768 (16)	51509	23	51301–51717	1.97	363 (4)
1624−4721	0.448 723 248 57 (7)	4.148 (9)	51683	21	51411–51954	2.32	364 (5)
1626−4537	0.370 141 128 114 (9)	8.2788 (11)	51683	26	51411–51954	0.56	237.0 (7)
1627−5547	0.352 464 213 20 (7)	0.7377 (20)	51561	23	51686–52116	0.36	166.2 (9)
1628−4828	4.137 538 5239 (16)	17.53 (18)	51393	33	51040–51745	15.15	1209 (15)
1630−4719	0.559 071 333 02 (4)	14.178 (19)	51340	20	51158–51521	0.73	489.6 (16)
1633−4805	0.710 830 078 80 (16)	76.893 (16)	51588	27	51221–51955	4.93	1120 (9)
1635−4513	1.594 745 5499 (8)	3.6 (3)	51306	19	51089–51523	7.89	416 (5)
1635−4944	0.671 964 199 32 (9)	8.79 (3)	51447	25	51216–51677	2.71	474 (6)
1636−4803	1.204 643 8889 (3)	20.71 (15)	51299	16	51099–51499	3.39	503 (7)
1636−4933	0.430 366 558 00 (4)	1.506 (13)	51305	16	51089–51521	1.09	542.7 (15)
1637−4335	0.771 366 540 42 (18)	3.62 (3)	51707	26	51459–51955	4.51	608 (8)
1637−4642	0.154 027 427 712 (10)	59.204 (8)	51571	31	51393–51747	0.91	417.0 (12)
1637−4721	1.165 741 386 60 (20)	4.44 (13)	51296	15	51099–51492	2.48	448 (7)
1638−4344	1.121 944 193 55 (7)	0.025 (16)	51707	25	51459–51955	1.43	237 (3)
1638−4608	0.278 137 287 280 (6)	51.5041 (9)	51480	32	51215–51745	0.56	424.3 (8)
1638−5226	0.340 502 709 437 (6)	2.650 (4)	52145	18	51946–52344	0.59	170.1 (15)
1639−4359	0.587 558 977 69 (4)	0.015 (15)	51490	19	51301–51678	0.76	258.9 (16)
1640−4648	0.178 352 043 293 (13)	0.8061 (13)	51608	27	51244–51971	2.23	474 (3)
1640−4951	0.739 098 946 49 (3)	0.334 (5)	51486	33	51216–51754	0.98	411.4 (19)
1643−4522	1.347 899 472 90 (11)	8.283 (11)	51590	26	51222–51956	2.30	482 (4)
1643−4550	0.717 508 089 981 (16)	29.974 (3)	51685	27	51412–51956	0.64	450.8 (17)
1646−4308	0.840 679 9814 (3)	0.11 (8)	51757	20	51557–51956	8.85	595 (15)
1648−4458	0.629 631 535 67 (8)	1.854 (8)	51590	24	51222–51956	3.15	925 (6)
1648−4611	0.164 949 668 359 (9)	23.7456 (11)	51486	37	51216–51754	1.27	392.9 (17)
1649−4653	0.557 018 757 96 (10)	49.74 (5)	51294	16	51089–51498	2.27	332 (4)
1650−4126	0.308 917 678 787 (3)	0.0198 (4)	51685	26	51412–51956	0.22	251.5 (5)
1650−4341	0.309 398 365 719 (4)	0.01669 (19)	51737	20	51216–52257	1.04	673 (4)
1651−4519	0.517 443 20 409 (19)	8.19 (11)	51399	20	51216–51581	5.03	562 (6)
1653−4315	0.419 279 741 37 (9)	0.015 (4)	51587	38	50940–51554	8.61	337 (6)
1653−4854	3.059 509 6022 (5)	3.45 (11)	51708	27	51459–51956	4.21	354 (6)
1654−4140	1.273 945 125 77 (12)	0.13 (8)	51399	20	51216–51581	1.56	307 (3)
1657−4432	0.609 607 142 01 (4)	8.205 (5)	51685	25	51412–51956	1.54	375.3 (16)
1658−4306	1.166 449 0044 (5)	42.79 (6)	51451	23	51158–51743	7.46	845 (11)
1659−4316	0.474 381 434 61 (3)	0.171 (10)	51527	21	51299–51754	1.17	641 (2)
1659−4439	0.353 293 033 439 (15)	0.025 (3)	51685	28	51412–51956	1.33	535 (3)
1700−4939	0.578 363 439 22 (4)	1.078 (7)	51709	29	51460–51956	1.55	278 (3)
1702−3932	0.390 327 976 785 (19)	0.378 (5)	51709	29	51460–51956	1.32	530 (4)
1702−4128*	0.182 135 802 939 (6)	52.3448 (3)	51530	46	51089–51970	0.73	367.1 (7)
1702−4310*	0.240 523 864 77 (4)	223.7763 (18)	51597	37	51222–51970	2.39	377 (3)
1702−4428	2.123 505 7036 (6)	3.3 (4)	51400	16	51216–51583	3.10	395 (8)
1703−4442	1.747 293 489 43 (10)	14.300 (19)	51708	25	51459–51956	0.95	280.2 (19)
1705−3936	0.854 481 6637 (3)	19.27 (10)	51400	20	51216–51583	2.71	598 (5)
1705−3950	0.318 941 483 436 (14)	60.6031 (13)	51587	26	51217–51956	1.14	207.1 (13)
1705−4108	0.861 067 4067 (3)	34.71 (7)	51505	22	51299–51710	3.58	1077 (6)
1706−3839	0.586 287 401 34 (18)	3.00 (6)	51510	19	51301–51717	4.47	626 (7)
1706−4310	0.616 979 0441 (5)	6.506 (12)	51457	26	51687–52117	1.25	656.1 (18)
1707−4341	0.890 594 496 25 (3)	5.696 (4)	51708	25	51459–51956	0.51	398.2 (8)

Table 2 – *continued*

PSR J	Period, P (s)	$\dot{P}$ (10^{-15})	Epoch (MJD)	$N_{\rm toa}$	Data span (MJD)	Residual (ms)	DM ($\rm cm^{-3}$ pc)
1707−4729	0.266 473 637 43 (3)	1.5603 (6)	51496	26	51634–52117	0.26	268.3 (4)
1708−3827	1.225 781 9960 (7)	8.6 (5)	51401	17	51217–51585	5.82	788 (3)
1709−3626	0.447 857 060 325 (11)	2.2675 (13)	51400	27	51089–51710	0.70	393.6 (11)
1709−4342	1.735 898 235 (10)	0.8 (3)	51457	17	51687–52117	5.68	281 (14)
1710−4148	0.286 561 228 631 (15)	0.102 (4)	51335	20	51089–51580	1.10	461 (3)
1711−3826	0.465 364 645 59 (7)	7.413 (16)	51710	23	51463–51957	3.14	376 (7)
1713−3844	1.600 114 0423 (3)	177.41 (13)	51294	18	51090–51498	2.28	544 (5)
1715−3903	0.278 481 054 67 (3)	37.688 (14)	51399	18	51217–51580	1.06	313.1 (17)
1715−4034	2.072 152 9918 (3)	3.01 (6)	51482	21	51244–51719	2.38	254 (7)
1717−3737	0.682 418 626 53 (3)	5.293 (6)	51324	22	51090–51557	0.57	525.8 (12)
1717−3847	1.149 498 9184 (6)	0.82 (7)	51347	39	50941–51752	21.67	707 (6)
1717−4043	0.397 857 446 56 (3)	12.230 (13)	51388	22	51217–51580	0.76	452.6 (12)
1717−40433	0.349 928 508 07 (10)	1.75 (7)	51399	19	51217–51580	3.57	539 (5)
1719−4302	0.235 475 200 29 (3)	0.3921 (9)	51498	22	51633–52117	0.45	297.7 (6)
1725−3848	2.062 386 2583 (13)	23.0 (5)	51399	20	51217–51580	5.35	230 (11)
1725−4043	1.465 071 374 87 (9)	2.79 (3)	51728	22	51501–51955	1.16	203 (3)
1732−3729	2.184 001 347 08 (15)	1.30 (5)	51724	24	51492–51955	1.61	317 (3)
1736−3511	0.502 802 782 90 (13)	1.57 (8)	51386	19	51217–51555	2.02	106 (3)
1751−3323	0.548 225 110 488 (19)	8.897 (3)	51910	21	51632–52187	0.60	296.7 (6)
1829−0734	0.318 400 873 408 (18)	4.789 (9)	51947	17	51746–52148	0.87	316.8 (18)
1834−1710	0.358 306 049 291 (6)	0.0469 (12)	51892	25	51634–52149	0.23	123.8 (5)
1842−0905	0.344 642 757 467 (5)	10.4931 (5)	51805	26	51460–52149	0.30	343.3 (6)
1845−0743	0.104 694 545 163 (5)	0.3666 (11)	52010	17	51832–52186	0.03	281.0 (3)
1853+0545	0.126 400 229 1591 (13)	0.6111 (3)	51910	24	51633–52186	0.20	198.7 (5)
1857+0526	0.349 951 177 522 (4)	6.9311 (8)	51800	23	51413–52186	0.31	466.4 (12)
1904+0800	0.263 344 725 870 (9)	17.317 (3)	51911	21	51634–52187	0.57	438.8 (13)
1913+0446	1.616 129 871 71 (16)	278.904 (16)	51832	19	51632–52194	1.14	109.1 (17)

[B]binary pulsar, see Kaspi et al. (2000b) for binary parameters.

the following, we will consider this during our discussions, basing all of our values such as efficiencies, etc., on distances derived from the NE2001 model.

One can also consider the pulsar distances that would be needed for the γ-ray luminosity to be consistent with a typically observed efficiency, $0.01 \lesssim \eta_{f=1/4\pi} \lesssim 20$ per cent. Comparing these distances with an electron density model distance is useful, as it allows one to judge whether the uncertainties in the DM distance could accommodate for such variations. Similarly, one can assume beaming fractions different from $f = 1/4\pi$ to further explore the possibility of a genuine association.

Considering criteria such as the source separation, variability index, characteristic age, efficiency and distances, we finally derive a 'quality indicator', Q, for a proposed association. A '+' indicates a genuine or very likely association, while a '−' implies that the apparent association is almost certainly due to a chance alignment. Pairings marked with '+?' are plausible associations, while for '?' an association cannot be ruled out, but more sensitive instruments such as the Gamma-Ray Large Area Telescope (GLAST) are needed to study it further.

3.1.1 Parkes multibeam pulsars

The first entry of a PMPS pulsar in Table 4 lists a positional coincidence with 3EG J1013−5915. Camilo et al. (2001a) argued that PSR J1016−5857 is a plausible counterpart to that source and is possibly also associated with the SNR G284.4−1.8. Table 4 also shows that there are two more pulsars positionally coincident with the same EGRET source, but these are not likely to be physically related.

Two more EGRET sources potentially associated with PMPS pulsars have already been discussed in the literature. D'Amico et al. (2001) reported the discovery of PSR J1420−6048 and J1837−0604 and discussed a possible association with the two EGRET sources 3EG J1420−6038 and J1837−0606, both of which have a variability index consistent with known γ-ray pulsars. The first source has only one pulsar in its error box, PSR J1420−6048, and is likely to be associated with it as the characteristic age of the pulsar and the derived efficiency of $\eta_{f=1/4\pi} = 1$ per cent are approximately as expected for a γ-ray pulsar. Moreover, in a multiwavelength study, Roberts, Romani & Johnston (2001) presented pulsed X-ray data and discussed a possible relationship to SNR G313.6+0.3. These observations also suggest a smaller distance than that from the TC93 model, consistent with the NE2001 model distance.

The EGRET source 3EG J1837−0606 has two pulsars located in its error box, but only the spin-down luminosity of PSR J1837−0604 presented by D'Amico et al. (2001) is sufficient to explain the high-energy emission. With a nominal efficiency of 7 per cent, which is typical, this pulsar is likely to be a genuine counterpart. The other pulsar, J1837−0559, would require an unreasonably high efficiency, even when taking uncertainties in distance and beaming fraction estimates into account.

This paper reports the discovery of the 140-ms PMPS pulsar J1015−5719. As already discussed by Torres et al. (2001) using data made available prior to publication, this pulsar appears to be

Table 3. Derived parameters for 200 pulsars discovered in the Parkes Multibeam Pulsar Survey. We list the characteristic age, the surface magnetic dipole field strength, the rate of rotational energy loss, the distance derived from the DM and the TC93 model, the inferred z-height and the corresponding radio luminosity at 1400 MHz.

PSR J	$\log[\tau_c$ (yr)]	$\log[B_s$(G)]	$\log[\dot{E}$ (erg s^{-1}]	Dist. (kpc)	z (kpc)	Luminosity (mJy kpc^2)
0831−4406	6.59	11.81	33.22	12.7	−0.60	69.4
0834−4159	5.64	11.87	34.99	9.7	−0.18	18.0
0855−4644	5.15	11.84	36.03	9.9	−0.17	19.6
0855−4658	5.83	12.45	33.45	28.3	−0.59	184.2
0945−4833	6.04	12.11	33.72	2.7	0.17	2.9
1000−5149	6.63	11.70	33.36	2.3	0.11	1.4
1012−5830	5.95	12.96	32.18	5.3	−0.16	2.3
1013−5934	7.10	11.70	32.40	11.3	−0.51	242.6
1015−5719	4.59	12.46	35.92	4.9	−0.05	21.3
1019−5749	5.11	12.26	35.27	30.0	−0.36	720.0
1020−5921	5.69	12.86	32.93	2.6	−0.09	3.1
1022−5813	5.25	13.19	33.11	30.0	−0.44	180.0
1031−6117	6.43	11.87	33.39	30.0	−1.51	108.0
1035−6345	7.42	11.66	31.85	6.5	−0.54	10.2
1043−6116	5.64	12.24	34.23	18.1	−0.67	298.1
1052−5954	5.16	12.28	35.13	13.5	−0.09	27.3
1054−5943	6.13	12.08	33.59	6.8	−0.01	14.4
1055−6236	7.00	11.76	32.49	3.6	−0.17	1.6
1058−5957	7.17	11.81	32.04	7.1	−0.02	25.8
1103−6025	6.80	11.80	32.80	6.8	−0.04	7.9
1107−6143	5.26	13.23	33.02	13.7	−0.32	71.3
1117−6154	5.81	12.41	33.58	22.4	−0.40	341.2
1117−6447	7.88	11.73	30.79	27.1	−1.76	102.8
1124−5638	8.51	10.62	31.75	23.8	1.76	175.6
1124−6421	7.09	11.74	32.35	14.9	−0.79	42.2
1128−6219	8.87	10.88	30.50	30.0	−0.51	243.0
1130−5826	8.21	10.71	32.17	9.4	0.46	16.0
1132−5627	7.61	11.04	32.70	21.3	1.76	36.3
1141−6545	6.16	12.12	33.44	3.2	−0.21	1.0
1148−6415	7.28	12.48	30.50	9.1	−0.35	3.3
1152−6012	5.95	12.21	33.69	2.1	0.07	0.7
1154−6250	6.90	11.60	32.99	2.1	−0.02	0.3
1159−6409	8.64	11.11	30.50	6.0	−0.20	17.1
1201−6306	6.42	12.17	32.83	30.0	−0.41	117.0
1211−6324	7.43	11.53	32.10	12.3	−0.19	68.1
1214−5830	8.43	11.35	30.45	4.8	0.34	3.3
1222−5738	8.06	11.61	30.67	2.1	0.18	0.5
1225−6035	7.54	11.63	31.67	6.2	0.23	9.9
1231−6303	7.18	12.14	31.35	12.1	−0.06	219.6
1233−6312	6.11	12.30	33.18	20.5	−0.14	105.1
1233−6344	6.49	12.24	32.55	30.0	−0.49	72.0
1235−6354	7.31	11.36	32.66	27.0	−0.51	116.6
1237−6725	7.18	12.34	30.96	8.0	−0.64	23.1
1243−5735	7.97	11.29	31.48	19.2	1.76	51.6
1248−6344	5.27	12.27	34.93	24.0	−0.36	69.1
1249−6507	8.76	10.87	30.77	8.5	−0.33	7.3
1254−6150	6.67	11.54	33.59	2.2	0.04	0.8
1255−6131	6.42	12.22	32.74	7.4	0.17	7.0
1301−6310	5.27	12.79	33.88	2.1	−0.01	0.5
1302−6313	6.38	12.40	32.44	28.1	−0.19	142.1
1306−6242	6.42	12.39	32.39	22.7	0.05	72.1
1309−6526	8.54	10.94	31.06	19.9	−0.91	59.4
1314−6101	6.60	12.77	31.26	9.6	0.29	37.7
1319−6105	6.65	11.91	32.90	14.9	0.41	186.5
1322−6329	6.60	12.75	31.32	30.0	−0.43	153.0
1324−6146	6.38	12.34	32.56	30.0	0.45	657.0
1324−6302	7.60	12.20	30.40	11.0	−0.08	27.8

Table 3 – *continued*

PSR J	log[τ_c (yr)]	log[B_s(G)]	log[$\dot{E}$ (erg s^{-1}]	Dist. (kpc)	z (kpc)	Luminosity (mJy kpc^2)
1329−6158	5.86	12.87	32.54	8.1	0.08	14.4
1339−6618	7.40	11.65	31.90	7.6	−0.52	13.4
1344−6059	8.30	11.19	31.03	7.2	0.15	9.8
1354−6249	6.50	12.83	31.36	5.6	−0.08	7.6
1355−5925	6.51	12.44	32.12	8.4	0.36	39.1
1355−6206	9.15	10.47	30.76	8.0	−0.02	34.1
1403−6310	7.83	11.29	31.77	6.1	−0.15	24.5
1406−5806	6.87	11.63	33.00	6.7	0.39	37.9
1413−6141	4.13	12.99	35.75	11.0	−0.06	73.8
1418−5945	7.99	11.83	30.36	9.3	0.21	15.6
1420−6048	4.11	12.38	37.02	7.7	0.03	53.8
1424−5822	6.17	12.09	33.50	10.2	0.41	114.4
1424−6438	7.83	11.70	30.95	8.3	−0.52	16.6
1425−5723	8.41	10.95	31.29	1.5	0.08	0.5
1425−5759	7.18	11.87	31.92	10.8	0.49	10.5
1434−6006	6.21	11.99	33.62	7.2	0.03	12.6
1441−6137	7.71	11.82	30.94	4.4	−0.12	3.0
1449−5846	7.93	11.31	31.53	4.8	0.06	6.3
1452−6036	6.23	11.68	34.19	9.4	−0.19	124.5
1457−5900	6.81	12.37	31.63	4.2	0.00	126.4
1457−5902	5.70	12.35	33.91	11.3	−0.01	1149.2
1501−5637	7.86	11.57	31.15	6.8	0.21	9.6
1502−5828	5.46	12.70	33.68	12.2	0.03	74.4
1502−6128	7.00	12.03	31.95	7.9	−0.34	34.8
1504−5621	6.07	12.18	33.49	3.9	0.13	3.7
1509−5850	5.19	11.96	35.71	3.8	−0.04	2.2
1509−6015	6.40	11.93	33.33	13.7	−0.43	31.9
1511−5414	6.82	11.50	33.38	2.2	0.12	3.8
1511−5835	7.14	11.51	32.70	7.1	−0.06	25.2
1512−5431	7.23	12.30	30.95	6.6	0.34	16.6
1514−5925	5.91	11.82	34.54	4.5	−0.12	5.5
1515−5720	5.87	12.13	34.01	10.3	0.05	21.2
1522−5525	6.82	12.34	31.69	1.9	0.05	0.9
1524−5625	4.50	12.25	36.51	3.8	0.02	12.2
1524−5706	4.70	13.31	34.01	21.6	−0.07	191.3
1525−5417	6.00	12.61	32.79	6.0	0.22	6.5
1525−5605	7.58	11.26	32.32	6.8	0.07	11.5
1526−5633	7.59	11.29	32.25	6.4	0.01	4.6
1529−5355	7.24	11.93	31.65	7.8	0.27	22.2
1529−5611	6.50	12.27	32.46	3.8	0.01	2.0
1531−5610	4.99	12.04	35.96	3.1	0.00	5.8
1532−5308	8.03	11.24	31.47	4.5	0.19	5.0
1535−5450	5.80	12.46	33.49	4.6	0.06	3.6
1535−5848	6.25	11.97	33.57	3.1	−0.13	3.4
1537−5153	6.76	12.41	31.67	2.6	0.14	0.2
1538−5638	6.27	12.39	32.67	12.9	−0.20	46.6
1538−5750	8.28	11.17	31.11	2.4	−0.08	0.3
1539−5521	7.34	11.94	31.45	6.8	0.01	6.6
1541−5535	4.80	12.68	35.06	7.5	−0.04	12.2
1542−5303	5.39	12.99	33.24	6.0	0.17	12.7
1543−5013	6.00	12.41	33.17	6.8	0.44	7.8
1546−5302	5.89	12.42	33.38	6.1	0.14	11.9
1547−5839	6.81	11.58	33.22	7.2	−0.41	21.2
1548−4821	9.46	10.04	31.01	3.8	0.31	7.2
1548−4927	6.37	12.20	32.86	3.9	0.26	10.4
1549−5722	8.22	11.19	31.18	2.9	−0.12	0.9
1550−5242	5.82	12.57	33.22	6.7	0.14	14.2
1550−5317	7.38	12.07	31.11	8.4	0.11	28.5

Table 3 – *continued*

PSR J	log[τ_c (yr)]	log[B_s(G)]	log[$\dot{E}$ (erg s^{-1})]	Dist. (kpc)	z (kpc)	Luminosity (mJy kpc^2)
1554−5512	6.24	13.02	31.49	8.1	−0.17	7.1
1556−5358	6.18	12.51	32.62	7.0	−0.05	25.7
1602−4957	5.91	12.56	33.06	6.8	0.25	7.9
1610−5303	6.68	12.16	32.33	6.6	−0.12	33.1
1611−4811	7.02	12.21	31.55	5.4	0.23	2.3
1612−5136	6.31	12.14	33.12	18.1	−0.06	65.5
1614−5144	6.51	12.53	31.91	9.5	−0.10	14.6
1614−5402	8.50	11.12	30.79	7.0	−0.27	12.1
1615−5444	7.23	11.55	32.45	8.4	−0.41	41.5
1618−4723	6.21	11.81	33.97	3.4	0.13	11.7
1621−5243	6.88	11.73	32.77	7.8	−0.28	16.3
1624−4721	6.23	12.14	33.26	6.1	0.15	5.6
1626−4537	5.85	12.25	33.81	5.4	0.22	32.2
1627−5547	6.88	11.71	32.82	5.7	−0.47	20.8
1628−4828	6.57	12.94	30.99	14.3	0.04	59.3
1630−4719	5.80	12.45	33.51	6.7	0.09	20.6
1633−4805	5.17	12.87	33.93	11.9	−0.02	32.6
1635−4513	6.85	12.38	31.54	7.0	0.18	12.1
1635−4944	6.08	12.39	33.06	8.8	−0.24	31.3
1636−4803	5.96	12.70	32.67	6.5	−0.06	46.9
1636−4933	6.66	11.91	32.87	11.2	−0.30	56.4
1637−4335	6.53	12.23	32.49	30.0	1.20	162.0
1637−4642	4.62	12.49	35.81	5.8	0.03	26.0
1637−4721	6.62	12.36	32.04	5.9	−0.01	14.8
1638−4344	8.85	11.23	29.84	5.1	0.18	4.4
1638−4608	4.93	12.58	34.98	5.8	0.06	11.3
1638−5226	6.31	11.98	33.42	4.9	−0.32	14.3
1639−4359	8.79	10.98	30.47	5.2	0.17	25.3
1640−4648	6.54	11.58	33.75	6.1	−0.02	9.6
1640−4951	7.54	11.70	31.51	10.6	−0.41	16.9
1643−4522	6.41	12.53	32.13	6.2	0.04	4.2
1643−4550	5.58	12.67	33.51	5.9	0.01	11.8
1646−4308	8.08	11.49	30.86	11.0	0.26	39.9
1648−4458	6.73	12.04	32.47	9.9	0.00	53.8
1648−4611	5.04	12.30	35.32	5.7	−0.08	18.9
1649−4653	5.25	12.73	34.06	5.6	−0.14	9.8
1650−4126	8.39	10.90	31.42	5.1	0.18	7.4
1650−4341	8.47	10.86	31.35	8.1	0.07	17.1
1651−4519	6.00	12.32	33.37	7.3	−0.09	28.7
1653−4315	8.65	10.90	30.90	5.1	0.03	13.9
1653−4854	7.15	12.52	30.68	13.7	−0.78	33.8
1654−4140	8.19	11.61	30.39	5.2	0.11	18.8
1657−4432	6.07	12.35	33.16	5.6	−0.10	11.8
1658−4306	5.64	12.85	33.03	9.6	−0.04	73.7
1659−4316	7.64	11.46	31.80	7.9	−0.08	13.2
1659−4439	8.35	10.98	31.35	9.2	−0.22	35.4
1700−4939	6.93	11.90	32.34	14.5	−1.15	35.7
1702−3932	7.21	11.59	32.40	9.7	0.24	28.2
1702−4128	4.74	12.49	35.53	5.2	0.01	29.5
1702−4310	4.23	12.87	35.80	5.4	−0.08	21.3
1702−4428	7.01	12.43	31.13	7.0	−0.21	18.9
1703−4442	6.29	12.70	32.02	5.3	−0.18	6.0
1705−3936	5.85	12.61	33.09	8.4	0.12	11.4
1705−3950	4.92	12.65	34.87	3.9	0.05	22.3
1705−4108	5.59	12.74	33.33	11.9	−0.01	708.1
1706−3839	6.49	12.13	32.77	12.2	0.28	29.8
1706−4310	6.18	12.31	33.04	13.5	−0.32	51.0
1707−4341	6.39	12.36	32.50	8.0	−0.27	29.5
1707−4729	6.43	11.81	33.51	10.6	−0.77	213.5
1708−3827	6.35	12.52	32.27	17.6	0.35	130.1

Table 3 – *continued*

PSR J	log[τ_c (yr)]	log[B_s(G)]	log[$\dot{E}$ (erg s^{-1}]	Dist. (kpc)	z (kpc)	Luminosity (mJy kpc^2)
1709−3626	6.50	12.01	33.00	8.9	0.33	46.4
1709−4342	7.54	12.08	30.78	5.5	−0.21	4.2
1710−4148	7.65	11.24	32.23	6.9	−0.14	14.7
1711−3826	6.00	12.27	33.46	5.2	0.05	4.3
1713−3844	5.16	13.23	33.23	6.5	0.02	11.0
1715−3903	5.07	12.52	34.84	4.8	−0.03	10.6
1715−4034	7.04	12.40	31.13	4.6	−0.10	34.2
1717−3737	6.31	12.28	32.82	6.3	0.02	27.5
1717−3847	7.35	11.99	31.33	9.5	−0.08	27.2
1717−4043	5.71	12.35	33.88	9.0	−0.27	43.7
1717−40433	6.50	11.90	33.21	11.4	−0.31	53.3
1719−4302	6.98	11.49	33.07	9.4	−0.55	33.0
1725−3848	6.15	12.84	32.01	4.5	−0.14	2.8
1725−4043	6.92	12.31	31.54	4.8	−0.24	7.8
1732−3729	7.43	12.23	30.69	6.2	−0.24	11.9
1736−3511	6.71	11.95	32.69	2.7	−0.08	1.3
1751−3323	5.99	12.35	33.33	9.3	−0.55	111.7
1829−0734	6.02	12.10	33.77	5.5	0.14	13.4
1834−1710	8.08	11.12	31.60	3.5	−0.26	12.5
1842−0905	5.72	12.28	34.01	7.4	−0.28	44.4
1845−0743	6.66	11.30	34.10	5.8	−0.23	92.4
1853+0545	6.52	11.45	34.08	4.8	0.17	36.4
1857+0526	5.90	12.20	33.81	11.4	0.24	85.8
1904+0800	5.38	12.33	34.57	9.2	0.14	30.5
1913+0446	4.96	13.33	33.42	3.4	−0.17	5.6

a plausible counterpart to the non-variable EGRET source 3EG J1014−5705. The computed γ-ray efficiency is consistent with values for γ-ray pulsars, i.e. $\eta_{f=1/4\pi} = 7.5$ per cent.

The PMPS pulsar J1314−6101 is located on the edge of the error box of 3EG J1308−6112. Its DM distance of 9.6 kpc as derived by the Taylor & Cordes (1993) model is reduced to 6.1 kpc in the NE2001 model. Nevertheless, the observed spin-down luminosity is so small that the pulsar needs to be at a distance of only 50 pc to have a γ-ray efficiency of even 20 per cent. In fact, the very large variability index of $V = 4.61$ rules out almost certainly an identification of this EGRET source with a γ-ray pulsar at all.

Sturner & Dermer (1995) proposed that 3EG J1410−6147 may be associated with SNR G312.4−0.4. The variability index of this EGRET source is consistent with observed pulsar properties, and indeed, there are two PMPS pulsars located in the 95 per cent error box of the source (see Table 4 and Manchester et al. 2002). Both pulsars have also been considered by Torres et al. (2001) and more recently also by Doherty et al. (2003). PSR J1412−6145 could only be consistent with the EGRET source if the distance or the beaming fraction were severely overestimated. An error in distance by a factor of 4 or so would make an association barely acceptable, but even in the improved NE2001 model the distance is only reduced from 9.3 to 7.8 kpc. A more plausible counterpart seems to be PSR J1413−6141, the discovery of which is reported in this paper with a very young characteristic age of only 14 kyr. Manchester et al. (2002) also discussed a suggestive relationship of this pulsar with SNR G312.4−0.4. Doherty et al. (2003) recently addressed this question in a detailed multiwavelength study. They argue that it was PSR J1412−6145 that was formed in the explosion creating SNR G312−0.4, while none of the two pulsars is related to the EGRET source. Indeed, the NE2001 distance needs to be overestimated, to make PSR J1413−6141 a plausible counterpart to 3EG J1410−6147. More sensitive gamma-ray observations are needed to settle this question.

The error box of 3EG J1639−4702 contains a total of five known pulsars. The discoveries and timing parameters for three of them, PSRs J1637−4642, J1637−4721 and J1640−4648, are presented in this work. Only PSR J1637−4642 has a spin-down luminosity consistent with the EGRET flux density, making it a possible counterpart. This source would have a γ-ray efficiency of about $\eta \sim 15$ per cent at its NE2001 distance. We note that the variability index would be somewhat high for 3EG J1639−4702 to be a γ-ray pulsar. A fifth, relatively young PMPS pulsar has been discovered in the same error box and appears to be closest to the nominal EGRET position. Named according to the current, preliminary timing solution, PSR J1638−4715, however, exhibits parameters that seem to exclude its identification as a gamma-ray pulsar.

Two new pulsars presented in this paper, PSRs J1713−3844 and J1715−3903, both reside in the error box of 3EG J1714−3857. The latter pulsar is a possible counterpart but only if its DM distance is overestimated by a factor of 2–3. However, the new NE2001 distance estimate agrees well with the previous TC93 value. Interestingly, PSR J1713−3844 is also located close to SNR G347.3−0.5 for which a distance of ∼6 kpc is estimated (Slane et al. 1999). This distance is very close to the estimated pulsar distance but is too large to make the pulsar simultaneously associated with the EGRET source. The SNR harbours a compact central source detected in the X-ray range, the position of which is not consistent with any of the PMPS pulsars. Recently, in a targeted search Crawford et al. (2002) discovered a weak 392-ms radio pulsar, PSR J1713−3949, which was initially considered to be a possible counterpart. The current

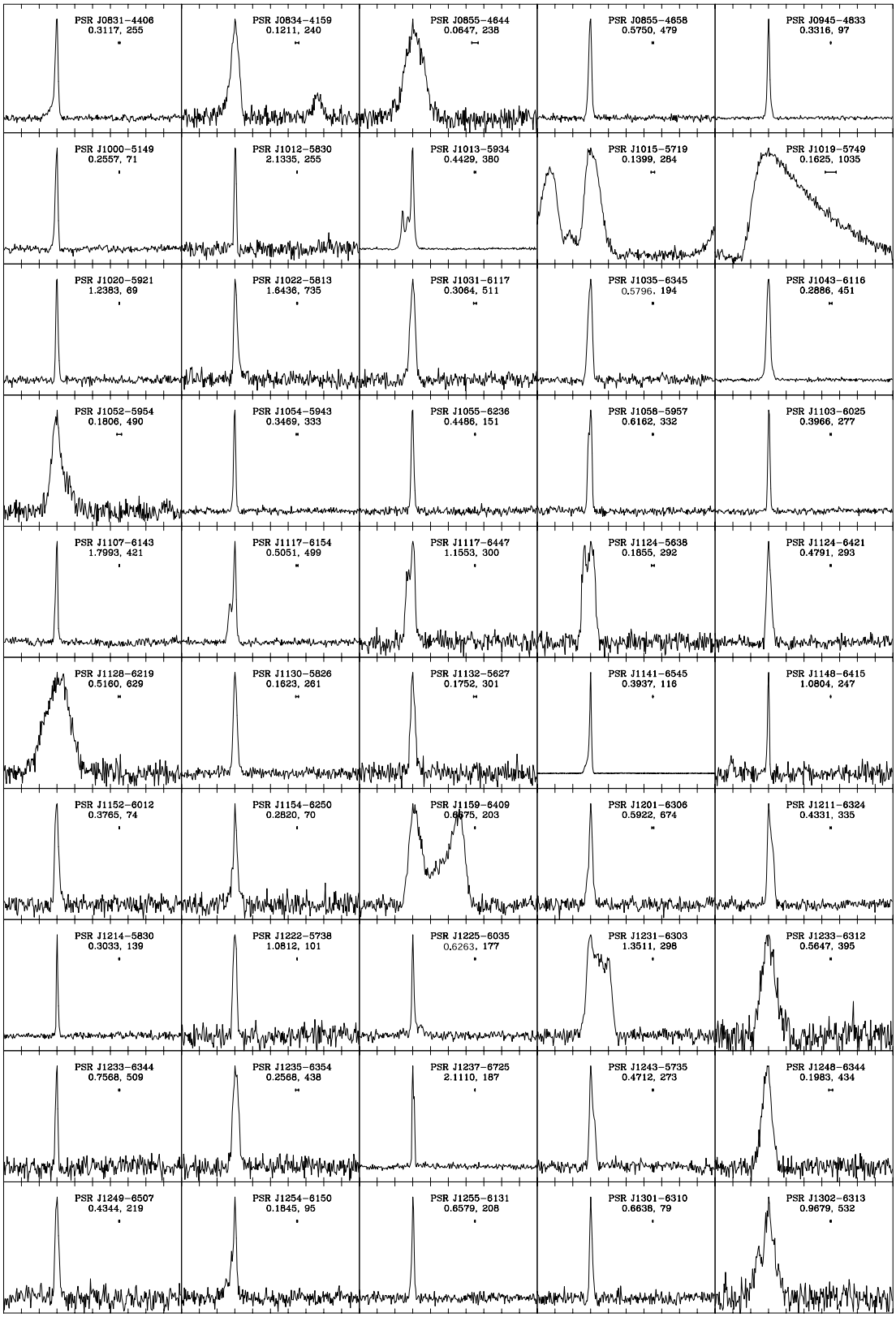

Figure 1. Mean pulse profiles at 1374 MHz for 200 pulsars discovered in the Parkes Multibeam Survey. The highest point in the profile is placed at phase 0.3. For each profile, the pulsar Jname, pulse period and dispersion measure are given. The small horizontal bar under the period indicates the effective resolution of the profile, including the effects of interstellar dispersion.

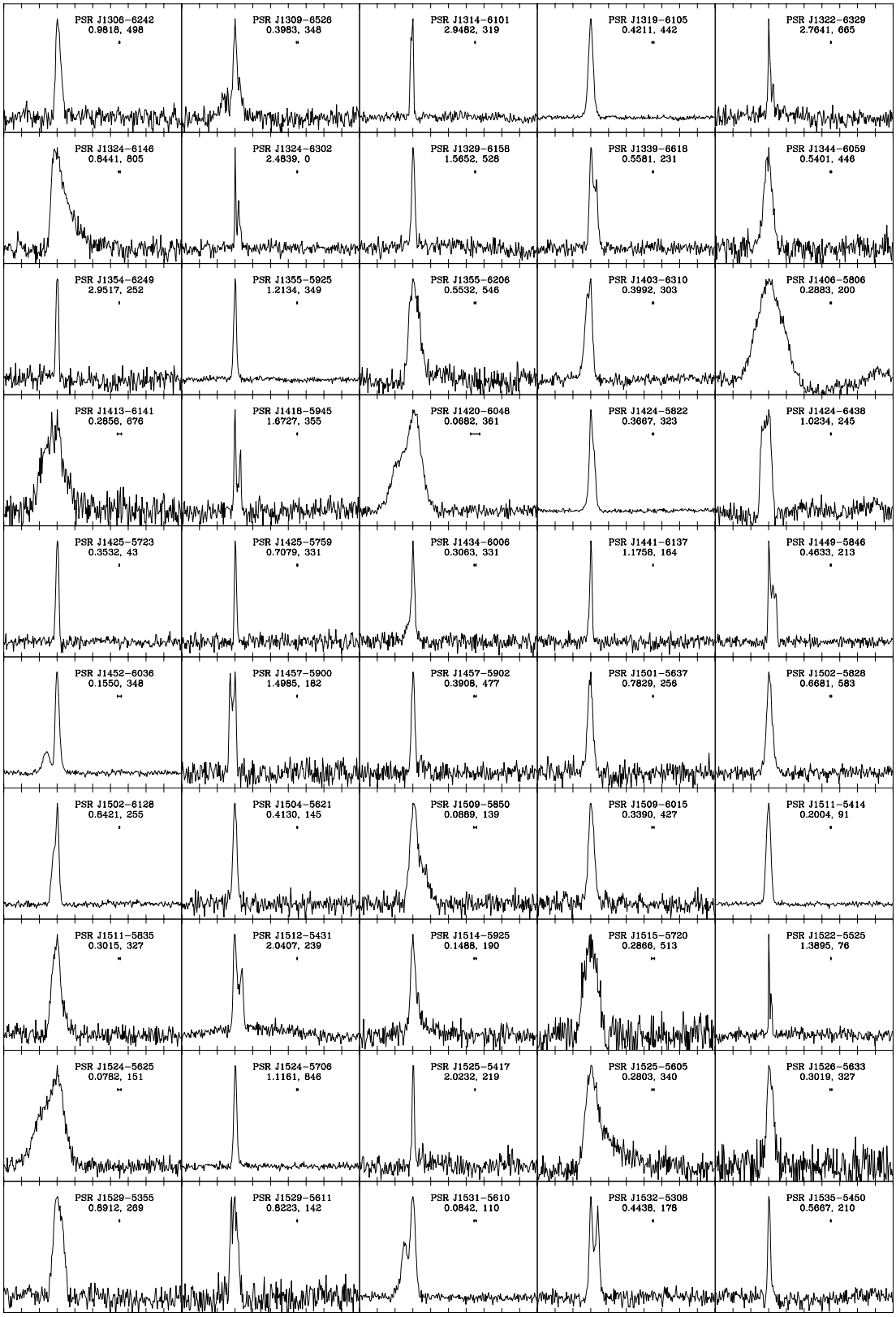

Figure 1 – *continued*

timing solution, however, places the source just outside the EGRET error box (i.e. $\Delta\Phi/\theta_{95} = 1.6$) and also suggests that this source is not consistent with the X-ray source either (Crawford, private communication).

The error boxes of the EGRET sources 3EG J1638−5155, J1704−4732, J1736−2908, J1741−2050, J1746−1001, J1824−1514, J1826−1302, J1837−0423, J1837−0606 and J1850−2652 all contain pulsars. These pulsars were either dis-

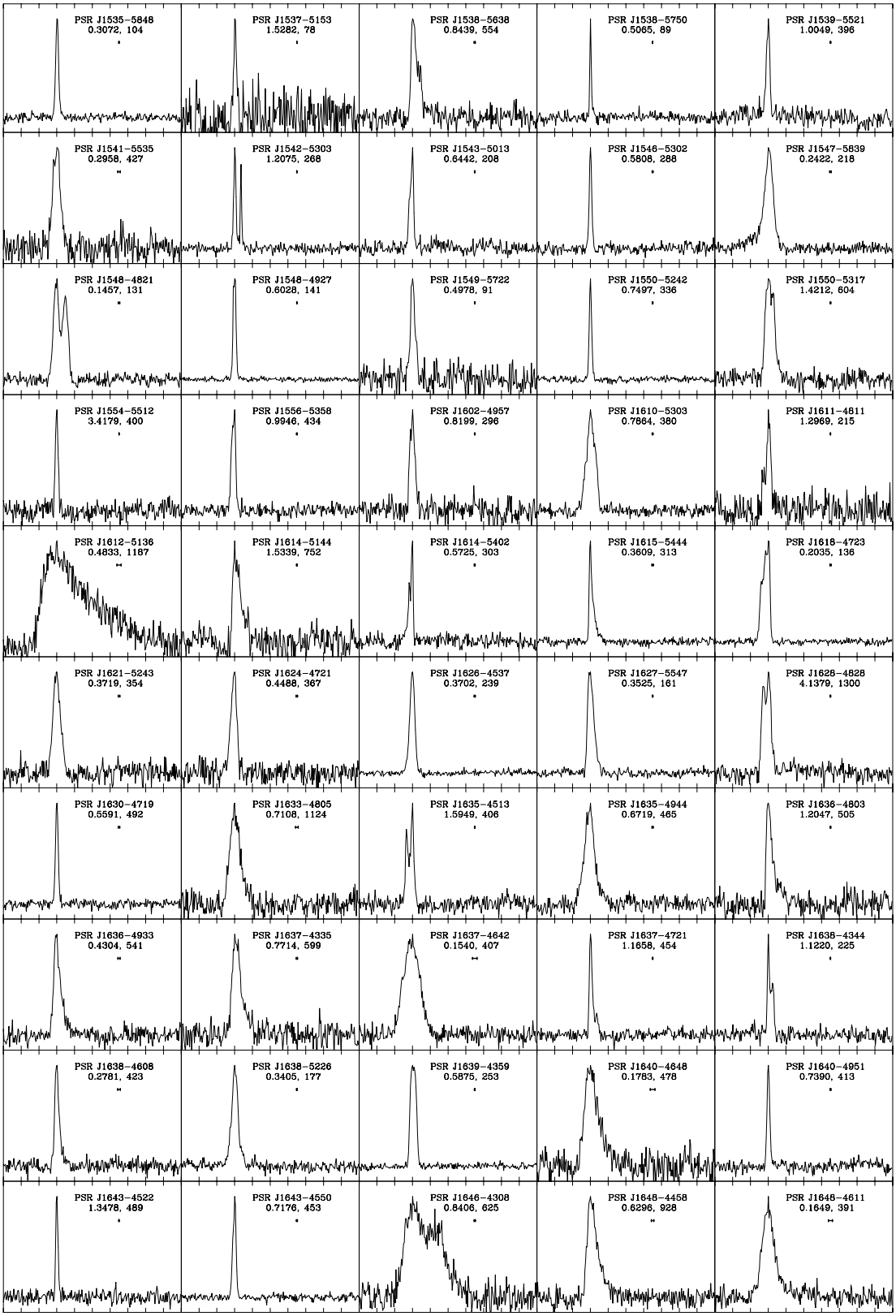

Figure 1 – *continued*

covered in the PMPS, previously known or recently discovered in the Swinburne Intermediate Latitude survey (Edwards et al. 2001). For the PMPS pulsars, parameters have already been presented here (PSRs J1638−5226, J1707−4729), in Paper II (PSRs J1823−1526, J1826−1526, J1838−0453, J1837−0559, J1837−0604) or will be presented in a forthcoming Paper IV (PSR J1736−2843, J1824−1505). None of the pulsars in the error boxes of these EGRET sources has parameters that suggest a physical

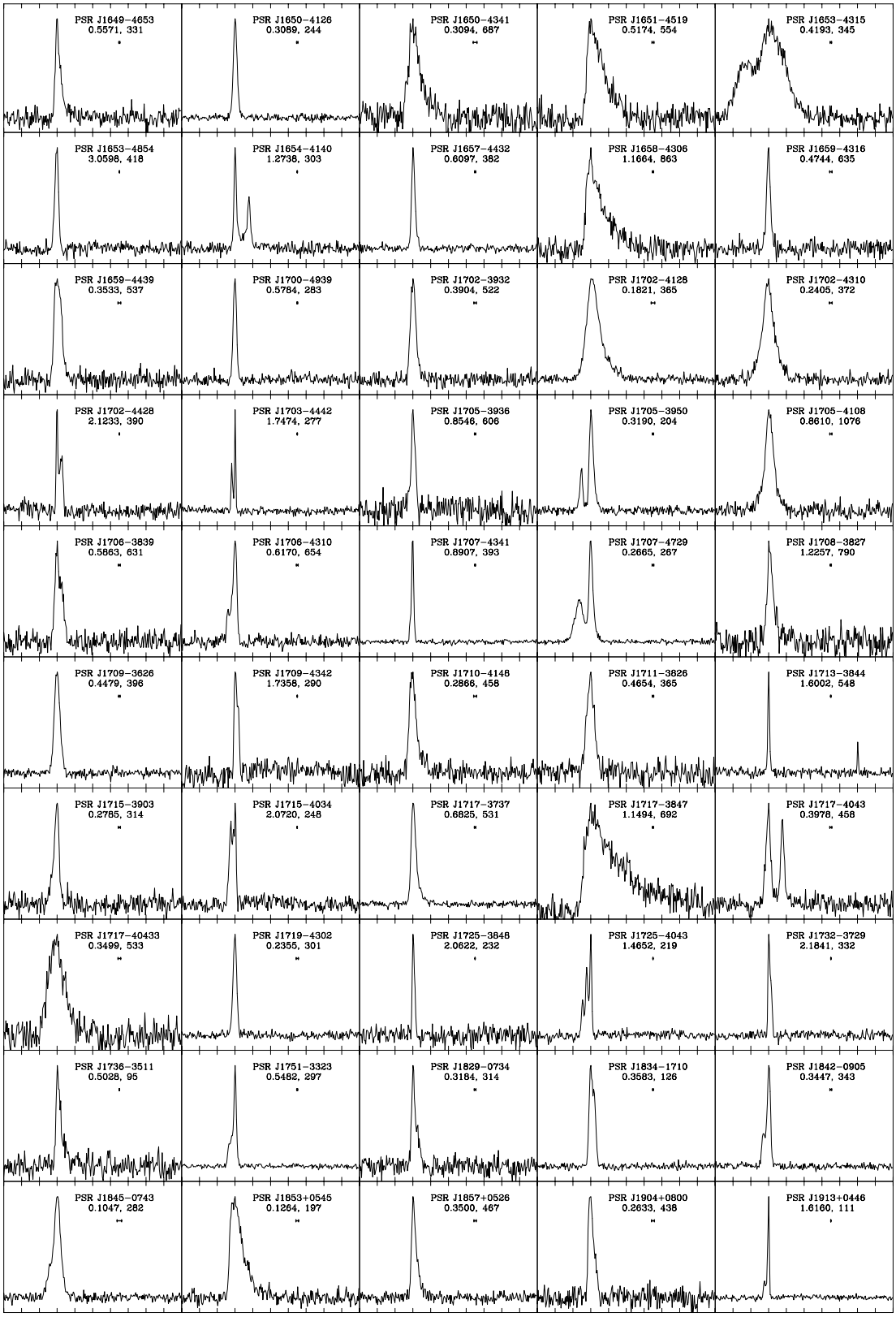

Figure 1 – *continued*

relationship with an EGRET source. A possible exception may be PSR B1823−13, positionally coincident with 3EG J1826−1302, which would have a very reasonable efficiency of just 2 per cent, but the variability index is very high.

Sturner & Dermer (1995) suggested that the EGRET source 3EG J1903+0550 is associated with SNR G40.5−0.5 (W44). Its error box contains four pulsars, three of which are multibeam discoveries, namely PSRs J1903+0609, J1905+0603 and J1905+0616. None

© 2003 RAS, MNRAS **342,** 1299–1324

Table 4. EGRET point sources as listed in the 3EG catalogue (Hartman et al. 1999) and radio pulsars positionally coincident with their error boxes. We list the EGRET source name (column 1), and its identification as listed in the catalogue (column 2). Assuming a spectral index of 2, a flux value $\bar{F}(E > 100\,\mathrm{MeV})$ in units of erg s^{-1} cm^{-2} is derived (column 3). A variability index, V, has been taken from McLaughlin (2001) (column 4), and the size of the 95 per cent error-box is quoted (column 5). Each EGRET point source is listed with pulsars (column 6) where the relative positional difference (column 7) is less than or equal to the size of the error-box. We also list those sources for which associations have been proposed in the literature. We quote the Taylor & Cordes (1993) model dispersion measure distances (column 8) and compare those to the new NE2001 (Cordes & Lazio 2002) distances (column 9), followed by the characteristic age (column 10). The NE2001 distance estimate is used to derive the $\dot{E}/d^2$ value (column 12) and the gamma-ray efficiency, η, for a beaming fraction of $1/4\pi$ (column 13), using the quoted spin-down luminosity (column 11). The likelihood of a genuine association is indicated by a '+', '−', '+?' or '?' in column 14. References to the pulsar and/or already proposed associations are given in column 15.

3EG J	ID	$\bar{F}$ (10^{-10} erg s^{-1} cm^{-2})	V	θ_{95} (deg)	PSR	$\Delta\Phi/\theta_{95}$	d_{TC93} (kpc)	d_{ne01} (kpc)	τ (kyr)	$\log[\dot{E}(\mathrm{erg\ s^{-1}})]$	$\log[\dot{E}/d^2\,(\mathrm{erg\ s^{-1}\ kpc^{-2}})]$	$\eta_{f=1/4\pi}$ (per cent)	Q	Ref
0222+4253	P	1.39 ± 0.22	0.13	0.31	J0218+4232	0.93	5.9	2.9	490 000	35.38	34.53	3.9	+	1
0500−0159	A	0.83 ± 0.17	3.63	0.75	J0459−0210	0.30	1.3	0.9	13 000	31.60	31.70	1800	−	2
0533−6916	G	1.06 ± 0.16	1.41	0.53	B0540−69	1.09	49.4∗	>47.8	1.8	38.12	34.82	1.5	−	3
					J0535−6935	0.64	49.4∗	>47.3	397	34.60	31.30	28.6	−	4
0534+2200	P	16.84 ± 0.35	0.50	0.05	B0531+21	1.23	2.5∗	1.7	1.3	38.64	38.04	0.02	+	5
0834−4511	P	62.10 ± 0.83	0.96	0.02	B0833−45	3.72	0.5∗	0.2	11	36.84	37.44	0.2	+	6
1013−5915	?	2.49 ± 0.45	0.15	0.72	B1011−58	0.41	10.2	7.9	21	33.11	31.30	11 500	−	7
					J1013−5934	0.45	11.3	8.5	12 580	32.48	30.48	69 000	−	III
					J1016−5857	0.67	9.3	8.0	21	36.42	34.61	5.8	+?	I, 8
1014−5705	?	2.53 ± 0.48	0.55	0.67	J1015−5719	0.44	4.9	5.1	39	35.92	34.50	7.5	+?	III, 9
1048−5840	?	4.60 ± 0.50	0.01	0.17	B1046−58	0.90	3.0	2.7	20	36.30	35.44	1.6	+	10, 20
1058−5234	P	2.48 ± 0.28	0.94	0.25	B1055−52	0.66	1.5	0.7	535	34.48	34.79	4.1	+	11
1102−6103	?	2.42 ± 0.46	2.38	0.61	J1104−6103	0.37	2.3	1.9	2263	33.54	33.00	250	−	12
					J1105−6107	0.62	7.1	5.0	63	36.40	35.00	2.3	+	10, 13
1308−6112	?	1.64 ± 0.45	4.61	0.71	J1314−6101	1.00	9.6	6.1	3891	31.30	29.70	3000 000	−	III
1410−6147	?	4.78 ± 0.65	0.72	0.36	J1412−6145	0.41	9.3	7.8	51	35.08	33.30	230	−	I, 14
					J1413−6141	0.75	11.0	10.1	14	35.75	33.74	84	*?*	III, 9, 14
1420−6038	?	3.33 ± 0.64	1.14	0.32	J1420−6048	0.53	7.7	5.6	13	37.00	35.50	1.0	+?	III, 15
1638−5155	?	2.23 ± 0.45	1.23	0.68	J1638−5226	0.79	4.9	3.3	2035	33.43	32.48	970	−	III
1639−4702	?	3.96 ± 0.65	1.88	0.56	B1636−47	0.52	7.3	6.5	195	34.08	32.48	1300	−	7
					J1637−4642	0.83	5.8	5.1	41	35.81	34.39	15.2	?	III, 9
					J1637−4721	0.81	5.9	5.3	4156	32.00	30.60	94 000	−	III
					J1638−4715†	0.46	6.7	6.1	59	33.56	32.00	3800	−	IV
					J1640−4648	0.65	6.1	5.5	3506	33.75	32.30	2030	−	III
1704−4732	?	1.53 ± 1.53	7.73	0.66	J1707−4729	0.71	10.5	6.2	2706	33.52	31.95	1660	−	III
1710−4439	P	8.35 ± 0.46	0.03	0.09	B1706−44	2.26	1.8	2.3	18	36.52	35.81	1.2	+	16
1714−3857	?	3.25 ± 0.48	2.27	0.51	J1713−3844	0.59	6.5	5.9	143	33.23	31.70	7630	−	III, 9
					J1715−3903	0.48	4.8	4.1	117	34.84	33.61	74.3	−	III, 9
1736−2908	?	2.46 ± 0.44	7.73	0.62	J1736−2843	0.67	7.4	5.8	3400	30.60	29.00	18 000	−	IV
1741−2050	?	1.79 ± 0.29	4.24	0.63	J1741−2019	0.84	2.0	1.72	3805	31.00	30.48	46 000	−	17
1746−1001	?	1.47 ± 0.26	9.30	0.76	J1745−0952	0.84	2.4	1.8	3200 000	32.70	32.20	900	−	18
1824−1514	?	2.62 ± 0.48	3.59	0.52	B1822−14	0.89	5.4	5.0	195	34.61	33.21	154	−	19
					J1823−1526	0.77	9.3	8.1	6092	31.60	29.78	420 000	−	II
					J1824−1505	0.38	8.6	7.5	4687	32.90	31.00	18 000	−	IV
					J1826−1526	0.75	10.9	8.2	5581	32.90	31.00	22 000	−	II

Table 4 – *continued*

3EG J	ID	$\bar{F}$ (10^{-10} erg s^{-1}cm^{-2})	V	θ_{95} (deg)	PSR	$\Delta\Phi/\theta_{95}$	$d_{\rm TC93}$ (kpc)	$d_{\rm ne01}$ (kpc)	τ (kyr)	$\log[\dot{E}(\rm erg\ s^{-1})]$	$\log[\dot{E}/d^2\,(\rm erg\ s^{-1}\ kpc^{-2})]$	$\eta_{f=1/4\pi}$ (per cent)	Q	Ref
1826−1302	?	3.45 ± 0.54	5.89	0.46	B1823−13	1.17	4.1	3.9	21	36.46	35.28	1.8	?	19, 20
1837−0423	?	1.42 ± 1.42	9.85	0.52	B1834−04	0.55	4.6	4.9	3381	33.18	31.78	2200	–	19
					J1838−0453	0.98	8.3	8.1	52	34.92	33.11	110	–	II
1837−0606	?	3.69 ± 0.59	2.81	0.19	J1837−0559	0.74	5.0	5.4	964	34.20	32.78	650	–	II
					J1837−0604	0.90	6.2	6.4	34	36.30	34.69	7.2	+?	II, 15
1850−2652	?	0.48 ± 0.19	4.50	1.00	J1852−2610	0.88	2.2	1.8	610 000	32.00	31.48	1600	–	2
1856+0114	?	5.02 ± 0.64	1.32	0.19	B1853+01	0.30	2.8	3.1	20	35.63	34.65	10.5	?	19, 21
1903+0550	?	4.62 ± 0.66	3.14	0.64	B1900+05	0.39	3.9	4.7	917	33.08	31.70	8100	–	22
					J1903+0609	0.31	8.1	7.1	308	34.15	32.48	1600	–	IV
					J1905+0603	0.75	18.3	11.7	7807	32.60	30.48	150 000	–	IV
					J1905+0616	0.88	5.3	5.7	116	33.74	32.30	2600	–	II
2021+3716	?	4.40 ± 0.46	2.53	0.30	J2021+3651	1.38	19.2	12.4	17	36.53	34.34	18.9	+?	23
2227+6122	?	41.3 ± 6.1	0.19	0.49	J2229+6114	0.56	12.0	7.3	11	37.34	35.62	0.7	+	24

*Distance obtained by independent estimate, used for $\dot{E}/d^2$.
† Name and parameters based on prelimanary timing solution.
References. III – this work, I – Paper I, II – Paper II, IV – Parkes Pulsar, unpublished.
1. Kuiper et al. (2000), 2. D'Amico et al. (1998), 3. Manchester et al. (1993), 4. Crawford et al. (2001), 5. Staelin & Reifenstein (1968), 6. Large, Vaughan & Mills (1968), 7. Johnston et al. (1992), 8. Camilo et al. (2001a), 9. Torres et al. (2001), 10. Kaspi et al. (2000a), 11. Fierro et al. (1993), 12. Kaspi et al. (1996), 13. Kaspi et al. (1997), 14. Manchester et al. (2002), 15. D'Amico et al. (2001), 16. Thompson et al. (1992), 17. Edwards et al. (2001), 18. Edwards & Bailes (2001), 19. Clifton et al. (1992), 20. Merck et al. (1996), 21. Wolszczan, Cordes & Dewey (1991), 22. Hulse & Taylor (1974), 23. Roberts et al. (2002), 24. Halpern et al. (2001).

of the four pulsars has sufficient spin-down luminosity to explain an association with the EGRET source.

3.1.2 Pair statistics

Table 4 shows that the known population of pulsars includes about 48 pulsars that have positional coincidence with EGRET error boxes. Of these, we believe that 16 pulsar/EGRET pairs are genuine or plausible associations. Note that this number does not include Geminga and PSR B1951+32, which were not listed in Table 4. Geminga does not appear to be a normal radio pulsar (Kuzmin & Losovskii 1997; Malofeev & Malov 1997; McLaughlin et al. 1999), while PSR B1951+32 is probably detected in EGRET data but not associated with an EGRET point source (Ramanamurthy et al. 1995). Most of the suggestive associations can only be confirmed when more sensitive instruments such as GLAST become available to detect pulsed emission consistent with the radio pulsar period.

The number of radio pulsars detectable at high energies impacts the understanding of the magnetospheric emission processes. Many authors therefore have attempted to model the small-number statistics of the genuine EGRET detections (e.g. McLaughlin & Cordes 2000; Zhang, Zhang & Cheng 2000; Gonthier et al. 2002). These results are also used to forecast the number of γ-ray pulsars to be detected by GLAST. In the following we will try to answer the question of how many pulsar/EGRET source pairs are likely to occur by chance in the presently known catalogues, in a much simpler manner. This more model-free approach follows the procedure used by Lorimer, Lyne & Camilo (1998) to study the chance alignment of pulsar/supernova remnant pairs.

We study the normalized deviation of a pulsar from a given EGRET position, $\delta \equiv \Delta\Phi/\theta_{95}$, by deriving the distribution of δ that occurs by chance and comparing this directly with the observed distribution. For completely unrelated sets of pulsars and EGRET sources, the number of pairs occupying an annulus between δ and $\delta + d\delta$ is proportional to δ, regardless of the relative densities of pulsars and EGRET sources over the plane of the sky (see Lorimer et al. 1998). One can demonstrate this by applying systematic shifts to the positions of all known pulsars before recalculating the new resulting distribution of δ from this shifted population, which will produce different by-chance alignments. We follow the example of Lorimer et al. and perform this decoupling of pulsar and EGRET samples for systematic shifts of $\pm4^\circ$ and $\pm8^\circ$ in Galactic longitude. Note that shifts in Galactic longitude are chosen to avoid biases in the simulated samples due to the Galactic nature of radio and γ-ray pulsars. These shifts are small compared with changes in the density of both types of objects in the sky, but much larger than the typical error box of an EGRET point source. We plot the resulting distribution of the shifted sample as well as the observed distribution in Fig. 2. The distribution for the shifted sample shows the expected linear increase with position deviation as indicated by the solid line.

Inspecting Fig. 2 we note that there is an excess of observed pairs for $\delta \leqslant 1$. The observed pulsar sample produces 50 pairs positionally coincident with EGRET sources (including now Geminga and PSR B1951+32), while the fake shifted sample produces only 31 ± 6 pairs. Hence we have an excess of 19 ± 6 possible associations. This is larger than the number of fully established associations, but consistent with our derived number of 16 associations that we classified as '+', '+?' or '?' in Table 4.

We can consider this result as a good indication that many of the proposed but not yet fully established associations may indeed be

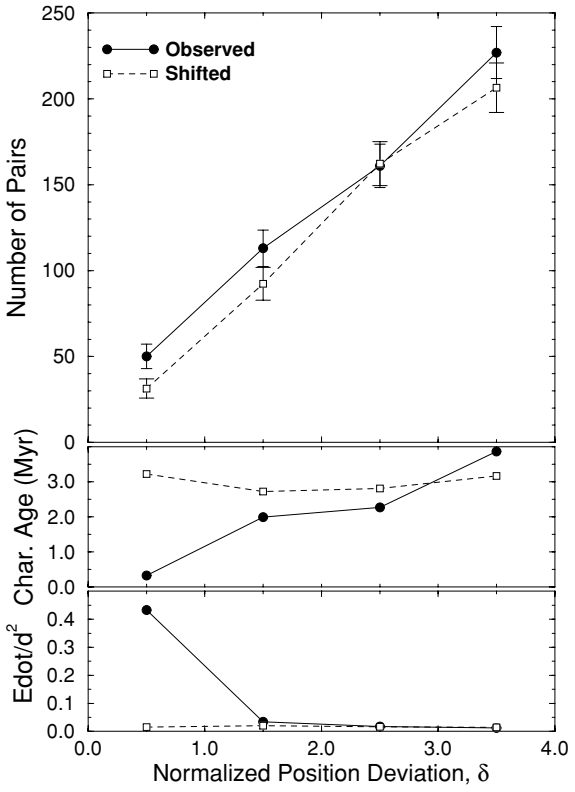

Figure 2. Top panel: number of EGRET source/pulsar pairs as found for the observed sample of pulsars, and a sample of pulsars shifted systematically in Galactic longitude, as a function of normalized position deviation. Points are plotted in the centre of the annulus intervals $\delta + \mathrm{d}\delta$ considered. Middle panel: median characteristic age of the pulsars in the corresponding pairs; bottom panel: median $\dot{E}/d^2$ of the pulsars in the corresponding pairs.

real. This view is supported by inspecting the median characteristic age and $\dot{E}/d^2$ for pairs in a given δ-interval: the pairs for $\delta \leqslant 1$ are much younger and have much larger spin-down fluxes (see Fig. 2 middle and bottom). Interestingly, inspecting the numbers derived to produce this Fig. 2, this trend continues, albeit with a much smaller difference in values, even for δ somewhat larger than unity. One can speculate as to whether this indicates a physical relationship between EGRET point sources and pulsars that lie just outside the nominal 95 per cent error box. Just such an example is the aforementioned PSR B1823−13. However, even when excluding this source from calculating the median $\dot{E}/d^2$, the resulting value is still significantly larger than that for larger δ or the shifted sample.

The results of our simple statistical analysis agree well with the conclusions of more complicated studies such as that of McLaughlin & Cordes (2000). Based on a likelihood analysis, they argued that about 20 unidentified EGRET sources are probably γ-ray pulsars. This estimate of 20 sources includes radio-quiet sources of Geminga type, of which a second one may have been identified (see Halpern et al. 2002). The similarity to our estimate of 19 ± 6 genuine associations with EGRET sources is therefore intriguing, even though the involved uncertainties are considerable.

In any case, it is certain that many more γ-ray pulsars will be detected with GLAST, and McLaughlin & Cordes, for instance, estimate up to 750 sources. While we can argue here only on statistical grounds, we can nevertheless expect that a number of those new radio pulsar/GLAST source associations will, in retrospect, also be found in the older EGRET/pulsar data.

Table 5. Young pulsars with spin parameters similar to the Vela pulsar. All sources selected have ages $10 \leqslant \tau_c \leqslant 100$ kyr and spin-down luminosities of $\dot{E} \geqslant 10^{36}$ ergs[1]. Pulsars marked with G are known to exhibit glitches, while sources labelled with E are or may be associated with EGRET point sources.

PSR	P (ms)	Age, τ_c (kyr)	$\dot{E}$ (10^{36} erg s^{-1})	Ref.	Notes
B0833−45	89.3	11	6.9	1	G, E
J0855−4644	64.7	141	1.1	III	
J0940−5428	87.5	42	1.9	I	
J1016−5857	107.4	21	2.6	2	G, E
B1046−58	123.7	20	2.0	3, 4	G, E
J1105−6107	63.2	63	2.5	5	G, E
J1112−6103	65.0	33	4.5	I	
J1301−6305	184.5	11	1.7	I	
B1338−62	193.3	12	1.4	7	G
J1420−6048	68.2	13	10.0	III, 8	E
J1524−5625	78.2	32	3.2	III	
J1531−5610	84.2	97	0.9	III	
B1706−44	102.5	18	3.4	3	G, E
J1718−3825	74.7	90	1.3	I	
B1727−33	139.4	26	1.2	3	G
J1747−2958	98.8	26	2.5	9	
B1757−24	124.9	16	2.6	7	G
B1800−21	133.6	16	2.2	10	G
J1809−1917	82.7	51	1.8	II	
B1823−13	101.5	21	2.9	10	G, E
J1828−1101	72.1	77	1.6	II	
J1837−0604	96.3	34	2.0	II, 8	
J1913+1011	35.9	169	2.9	I	
B1951+32	39.5	107	3.7	11	
J2021+3651	103.7	17	3.4	12	E
J2229+6114	51.6	11	22.0	13	E

References. III – this work, I – Paper I, II – Paper II, 1. Large et al. (1968), 2. Camilo et al. (2001a), 3. Johnston et al. (1992), 4. Kaspi et al. (2000a), 5. Kaspi et al. (1997), 6. Camilo et al. (2000), 7. Manchester, D'Amico & Tuohy (1985), 8. D'Amico et al. (2001), 9. Camilo et al. (2002a), 10. Clifton et al. (1992), 11. Kulkarni et al. (1988), 12. Roberts et al. (2002), 13. Halpern et al. (2001).

3.2 Vela-like pulsars

The archetypal young, energetic pulsar is PSR B0833−45 in the Vela supernova remnant. A number of other young pulsars share many properties with Vela, such as having detectable X-ray or γ-ray emission, being associated with pulsar wind nebulae, or being known to exhibit instabilities in their rotation ('glitches'). The PMPS has uncovered 12 more such Vela-like pulsars, which we will loosely define as sources with characteristic ages in the range $10 \lesssim \tau_c \lesssim 100$ kyr and spin-down luminosities $\dot{E} \gtrsim 10^{36}$ erg s^{-1}. The new sources almost double the number of known Vela-like pulsars, increasing it to a total of 26. All 26 sources are listed in Table 5 where we also quote corresponding references and indicate which pulsars are known to glitch. Glitch information is obtained from the work by Shemar & Lyne (1996), Camilo et al. (2000) and Wang et al. (2000) and references therein. As indicated, nine of these pulsars already appeared in Table 4 as genuinely or possibly related to EGRET point sources.

Radio continuum maps have been obtained and/or studied for a number of PMPS pulsars in Table 5. Crawford (2000) obtained radio maps with the Australia Telescope Compact Array (ATCA) for PSRs J0940−5428, J1112−6103, J1301−6305 and J1420−6048. The latter pulsar (D'Amico et al. 2001 and this work) is surrounded

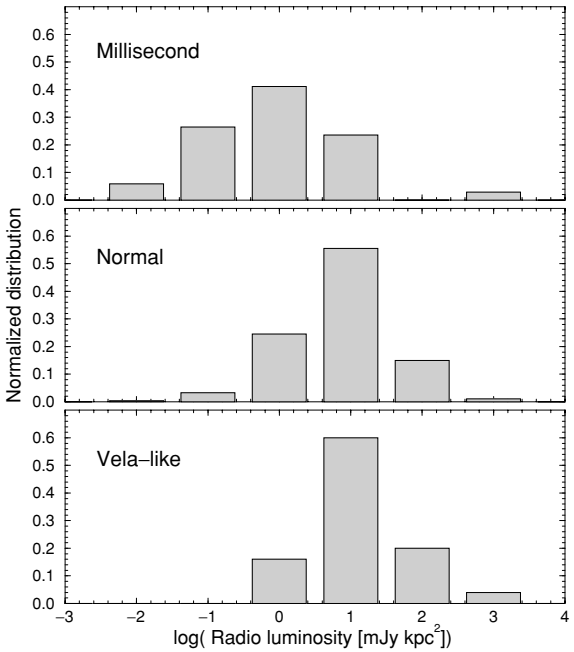

Figure 3. Observed distribution of radio luminosities measured at 1400 MHz for millisecond pulsars, 'normal' pulsars and 'Vela-like' pulsars.

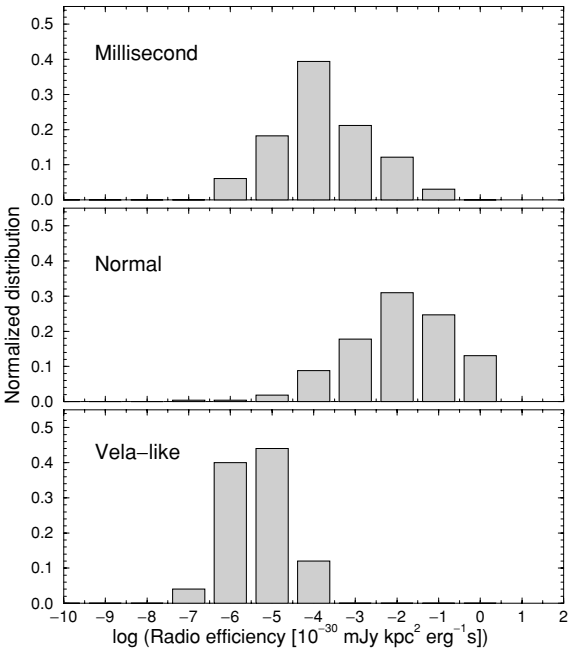

Figure 4. Observed distribution of radio efficiencies measured at 1400 MHz for millisecond pulsars, normal pulsars and Vela-like pulsars.

by a pulsar wind nebula that was studied in detail by Roberts et al. (1999, 2001). Manchester et al. (2002) used ATCA data and maps from the Molongo Galactic Plane Survey (Green et al. 1999) to search for supernova remnants associated with PMPS pulsars. Further results will be published elsewhere.

Using the radio luminosity at 1400 MHz, L_{1400}, Camilo et al. (2002b) pointed out that young pulsars ($\tau_c \lesssim 100$ kyr) are not particularly luminous by comparison with middle aged pulsars. We can also demonstrate this for the smaller sample of Vela-like pulsars as shown in Fig. 3. While Vela-like pulsars have a median log L_{1400} of 1.5, normal pulsars (here defined as being non-Vela-like and non-recycled pulsars) exhibit a median of 1.4. In contrast, recycled or millisecond pulsars appear to be less luminous (median 0.4), although this is to some extent due to selection effects as discussed in detail by Kramer et al. (1998).

We can also define an efficiency as a radio emitter by comparing radio luminosity to the spin-down luminosity, $\epsilon_{1400} \equiv L_{1400}/\dot{E}10^{-30}$ Jy kpc^2 erg^{-1} s. Obviously, since the radio luminosities are very similar for Vela-like pulsars compared with normal pulsars, while $\dot{E}$ is much larger, it is clear that Vela-like pulsars must be much less efficient radio pulsars. Indeed, as demonstrated in Fig. 4, the medians measured for the three distributions in log ϵ_{1400} are -4.8 for Vela-like pulsars, -1.3 for normal pulsars and -3.2 for millisecond pulsars, respectively. The result for millisecond pulsars has already been discussed by Kramer et al. (1998), whilst that for Vela-like pulsars clearly demonstrates that spin-down and radio luminosities are not correlated for non-recycled pulsars. It is interesting to note that when computing the log median efficiency for energetic pulsars with $\dot{E} \gtrsim 10^{36}$ ergs^{-1} but ages larger or smaller than adopted for Vela-like pulsars, log ϵ_{1400} is even lower with median -5.8. However, this latter sample contains both millisecond pulsars and very young pulsars such as the Crab.

The computed radio efficiency effectively assumes that all pulsars beam into the same solid angle. Manchester (1996) argued that young pulsars exhibit wider beams, which may lead to an underestimation of the efficiency for Vela-like pulsars. We estimate that this might account for a factor of 10–100, but it appears unlikely that it explains for the full difference in the efficiency to normal pulsars. We therefore conclude that this much enlarged sample of young energetic Vela-like pulsars clearly demonstrates that such pulsars lose more energy outside the radio band than normal pulsars, and that radio luminosity does not increase with larger available spin-down luminosity. Instead, it is possible that some saturation process is operating. We also note that apart from possible correlations with age, we have also tested for possible dependences of efficiency and luminosity on period, magnetic field at surface and light cylinder, as well as an accelerating potential above the polar caps. No correlation has been found.

4 PULSARS AS GALACTIC PROBES

Pulsars are superb objects with which to probe the Galactic structure. In particular, the pulsars discovered in the PMPS probe large distances and Galactic lines of sight, which had largely not been accessible previously.

For the first time, the spiral arm structure becomes clearly visible when studying the distribution of pulsars along Galactic longitudes. In order to demonstrate this, we consider pulsars with a characteristic age of less than 1 Myr. These pulsars are young enough to be found close to their birthplace, even with a mean velocity of about 450 km s^{-1} (Lyne & Lorimer 1994). In order to restrict ourselves to pulsars in the Galactic disc, we only show pulsars with Galactic latitude $|b| \leqslant 20^\circ$ in Fig. 5. The Galactic longitudes where our lines of sight become tangents to Galactic spiral arms as given by Georgelin & Georgelin (1976) (see also Cordes & Lazio 2002) are indicated and largely can be associated with individual peaks in the number distributions. Interestingly, the Galactic longitude interval $0^\circ \leqslant l < 4^\circ$ does not contain any pulsar with a determined characteristic age of less than 1 Myr. Whilst there are newly discovered pulsars in this interval for which the spin-down properties still have to be

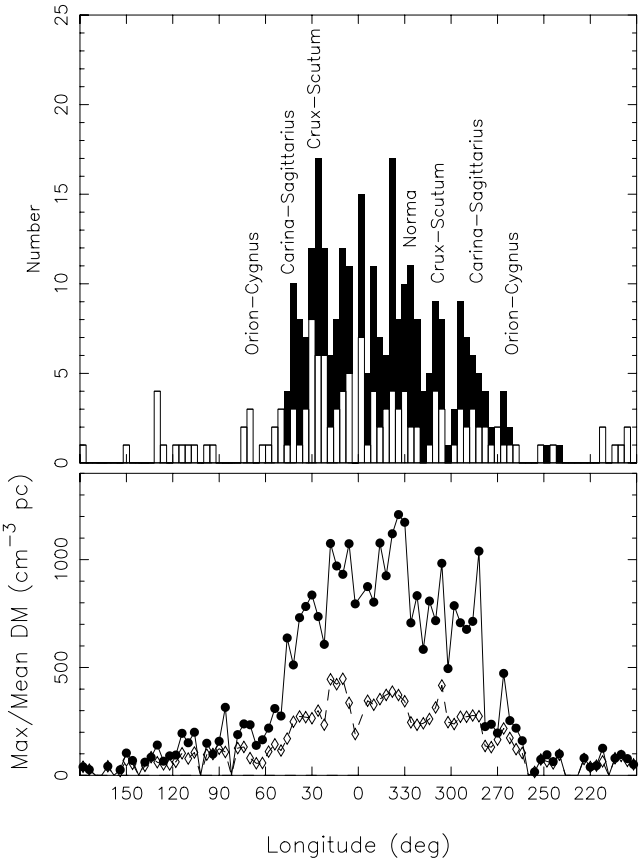

Figure 5. Top: number of pulsars with Galactic latitude $|b| \leqslant 20^\circ$ and a characteristic age of less then 1 Myr as a function of Galactic longitude. Filled bars mark the numbers of pulsars from the PMPS. The locations of the lines of sight tangential to the Galactic spiral arms are indicated. Bottom: maximum (filled circles) and mean (open diamonds) dispersion measures for these pulsars as a function of Galactic longitude.

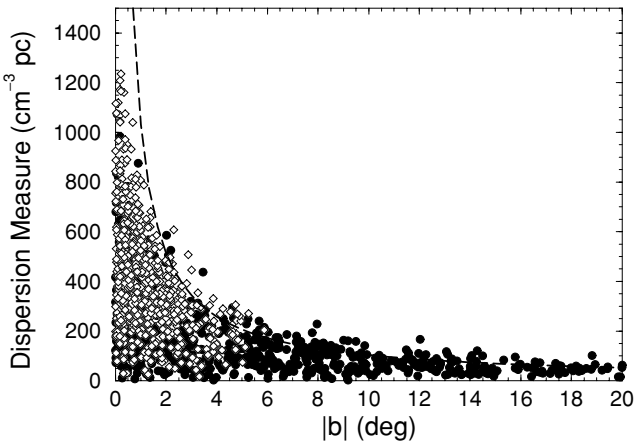

Figure 6. Observed dispersion measures as a function of the magnitude of Galactic latitude for PMPS pulsars (open diamonds) and all others (filled circles). The dashed line is described by DM $= 18/\sin|b|$ cm^{-3} pc.

determined, the known pulsars have ages larger than 1 Myr. In contrast, there are 15 pulsars with ages less than 1 Myr in the interval $356^\circ \leqslant l < 360^\circ$. The general dip in the distribution found around the Galactic Centre can in part be attributed to selection effects, i.e. enhanced scatter broadening, preventing the discovery of fast rotating pulsars in the innermost Galaxy for frequencies below about 5 GHz (see Cordes & Lazio 1997; Kramer et al. 2000). On-going population synthesis studies will investigate this effect further and results will be presented elsewhere.

We can expect that this structure in the number density should also be reflected in the observed dispersion measure distribution. In Fig. 5 we show the maximum and mean dispersion measure of all pulsars with $|b| \leqslant 20^\circ$. Indeed, individual spiral arms can be easily identified.

The dispersion measures of the newly discovered pulsars, as well as future measurements of scatter broadening times, obviously provide extremely valuable input to any modelling of the Galactic free electron density distribution. Despite the limitation of the survey to Galactic latitudes of $|b| \leqslant 5^\circ$, it also contributes significantly to studies of the scaleheight of the electron density above the Galactic plane, as we demonstrate in Fig. 6.

In the simplest model, we can describe the free electron distribution in a thin-slab model, with a constant electron density, n_e, and a height of $\pm H$ above and below the Galactic plane. It is then easy to show that the maximum possible dispersion measure along a Galactic latitude b, is given by $\mathrm{DM}_{\max} = n_e H/\sin b$. The envelope describing the data shown in Fig. 6 is given by $\mathrm{DM}_{\max} = 18/\sin|b|$ cm^{-3} pc, hence, $n_e\ H \sim 18$ cm^{-3} pc. With a canonical electron density of $n_e \sim 0.03$ cm^{-3}, we obtain a scaleheight of 600 pc. Obviously, in realistic models the electron density depends on the Galactocentric radius and z-height above and below the Galactic plane, This is the case for both the TC93 and NE2001 models, which use an 'outer thick component' deriving scaleheights of about 1 kpc.

Besides revealing the large-scale structure of the Milky Way, models of the free electron distribution are important in determining distance estimates for pulsars. A distance is derived by integrating the electron density in a given model along the line of sight towards the pulsar until the dispersion measure is reached. Such dispersion measure distances based on the TC93 electron density model are quoted in Table 3, consistent with Papers I and II. They were particularly important in Section 3.1, where we also used distances derived from the new NE2001 model as shown in Table 4. A reliable conversion from dispersion measure to distance and vice versa is therefore highly desirable.

The NE2001 model already incorporates a large number of dispersion measures from multibeam pulsars, so that with the new model fitting procedure developed by Cordes & Lazio (2002), we can expect a significant improvement of the model, in particular for distant pulsars. This is indeed the case, as we demonstrate in the following. The location of all known pulsars in the Galactic plane as derived from the TC93 model is shown in Fig. 7, whereas we applied the NE2001 model in Fig. 8. Newly discovered pulsars in the PMPS are marked as open diamonds. Once more, only pulsars with a Galactic latitude $|b| \leqslant 20^\circ$ are shown. The spiral arms in these figures are those used by Cordes & Lazio (2002) and are based on the model by Georgelin & Georgelin (1976), which was also used by Taylor & Cordes (1993). We point out that the apparent location of most pulsars along spiral arms has to be viewed with care since both TC93 and NE2001 incorporate explicitly this model of the spiral arm structure of the Galaxy, shapes and locations of which are derived from radio and optical observations. However, as pointed out by Taylor & Cordes (1993) and Cordes & Lazio (2002), and is clear from Fig. 5, the data make an inclusion of a spiral structure mandatory.

Limitations of the TC93 model are immediately visible from Fig. 7 since a number of pulsars are located far outside the Galaxy,

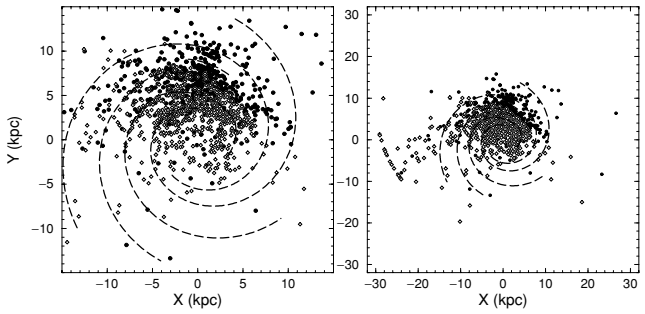

Figure 7. Location of known pulsars in the Galactic plane, $|b| \leqslant 20^\circ$, based on distance estimates derived from the TC93 model. The spiral arm structure as used in the electron density model is indicated. The left-hand panel shows the inner 15 kpc around the Galactic Centre, while the right-hand panel zooms out to demonstrate the existence of an artificial 30-kpc ring around the Sun [located at (0, 8.5)] caused by electron deficits in the TC93 model.

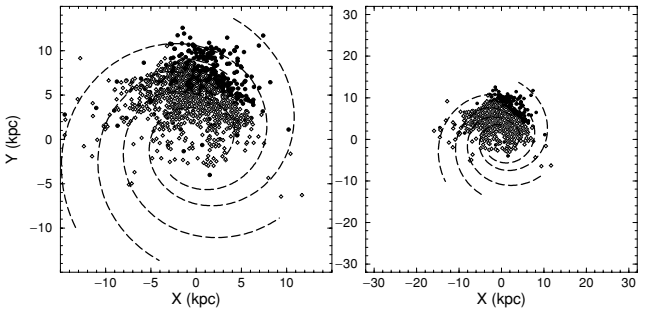

Figure 8. Location of known pulsars in the Galactic plane, $|b| \leqslant 20^\circ$, based on distance estimates derived from the NE2001 model. The right-hand panel demonstrates that the artificial 30-kpc ring around the Sun seen in the TC93 model has disappeared.

in particular along a semicircle with a radius of 30 kpc around the Sun. This artefact is caused by terminating the integration along the line of sight at that distance. The electron density is obviously underestimated towards these directions in the TC93 model. In contrast, the NE2001 model improves on the distribution significantly, also causing the 30-kpc circle to disappear. This goes along with a general decrease of pulsar distances, sometimes to a large extent as mentioned in Section 3.1.

A similar effect is seen in changes for the computed z-height above or below the Galactic plane. Figs 9 and 10 shows the magnitude of z-height computed from the TC93 and NE2001 models, respectively, as a function of the derived DM distance. Again, we restrict the sample shown to pulsars with $|b| \leqslant 20^\circ$. As before, the TC93 model runs out of electrons before the integration stops, producing artefacts in the resulting distribution. In stark contrast, the NE2001 model pulls the pulsars much closer towards the Sun and therefore also closer to the plane. There seems to be a paucity of pulsars in a region of large distances and large z-heights. We consider it unlikely that this can be attributed to a simple selection effect. In both cases, the vast majority of distant pulsars has been found in the PMPS. In spite of searching only latitudes of $|b| \leqslant 5^\circ$, this corresponds to a $|z|$-height of 1.3 kpc in 15-kpc distance and 2.6 kpc in 30-kpc distance, hence covering this area in principle.

A viable test for every electron density model is to check the existence of an (artificial) dependence of the computed z-height on the estimated distance. We make this test by computing the median of the absolute z-height in 2-kpc intervals for distances below

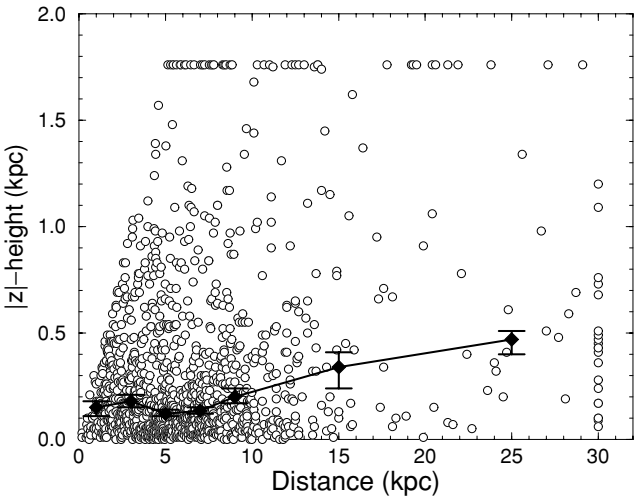

Figure 9. Location of known pulsars with $|b| \leqslant 20^\circ$ above and below the Galactic plane based on distance estimates derived from the TC93 model. The pulsars lying along a line of constant z-height and distance indicate an artefact in the model. Filled diamonds represent medians computed in 2-kpc intervals for distances below 10 kpc, and in 10-kpc intervals for larger distances, respectively. The error bars shown are obtained from the following reasoning: the median divides a sample of n pulsars, located in a given 2-kpc interval and sorted according to their $|z|$-height, into subsets of $n/2$ pulsars with $|z|$-values larger and smaller than the median, respectively, i.e. $|z|_{\rm median} = |z|_{n/2}$. We therefore estimate an uncertainty of $\pm\sqrt{n/2}$ for the number of pulsars in each $n/2$-subset. The error bars are then determined as the differences in $|z|$-height of the median and the $(\sqrt{n/2})$th element (counted from the median) in each subset.

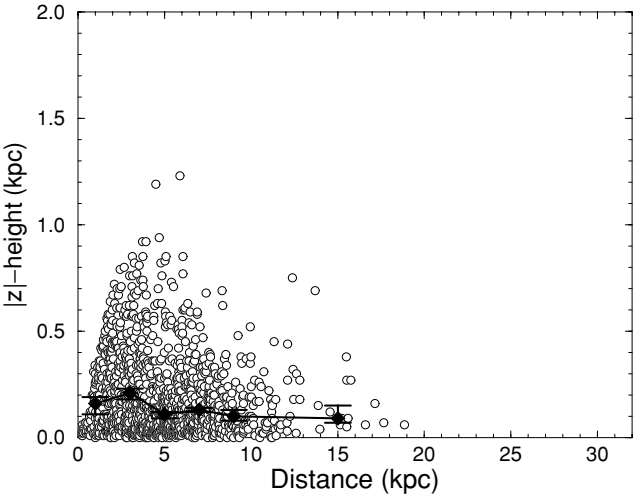

Figure 10. As in the previous figure, but with locations of known pulsars based on distance estimates derived from the NE2001 model.

10 kpc, and in 10-kpc intervals for distances beyond. These medians are shown as filled diamonds in Figs 9 and 10, centred on the corresponding intervals. Note that we choose the median rather than the mean to account for the demonstrated artefacts produced by the TC93 model.

The values for the TC93 model remain essentially constant up to 10 kpc. Beyond that distance, the small-number statistics results in large fluctuations with an apparent increase in the medians. In the

NE2001 model, the pulsars are significantly closer to the disc, and a slight trend is visible in the medians to decrease with distance.

In summary, the PMPS pulsars presented here and the associated papers provide an excellent tool for studying the structure of the Milky Way. The improved understanding of this structure feeds back into our understanding of pulsars. When, for instance, the distance of pulsars located in far Galactic regions identified above becomes more reliable, we can learn more concerning the luminosity of the pulsars, their distribution in the Milky Way and ultimately their population as a whole.

5 SUMMARY AND CONCLUSIONS

We have presented the parameters and pulse profiles for 200 pulsars newly discovered in the Parkes Multibeam Pulsar Survey. We paid particular attention to young pulsars for which we review the situation of possible associations with EGRET point sources. In a statistical analysis we showed that a number of new associations emerging from the Parkes Multibeam Pulsar Survey are likely to be genuine. We summarized the properties of the sample of Vela-like pulsars, of which many new examples are presented in this paper. We found that Vela-like pulsars are less efficient radio emitters than normal pulsars as their radio luminosity does not scale with the available spin-down luminosity. Finally, we demonstrated that the many new discoveries of distant pulsars in the Galactic plane help to significantly improve the model of the free electron distribution. For the first time, the spiral structure of the Galaxy is directly visible in the number distribution of pulsars along Galactic longitude.

In coming years we can expect further follow-up studies and investigations based on this unique sample of new pulsars.

ACKNOWLEDGMENTS

We gratefully acknowledge the technical assistance with hardware and software provided by Jodrell Bank Observatory, CSIRO ATNF, Osservatorio Astronomico de Bologna and Swinburne Centre for Astrophysics and Super-computing. The Parkes radio telescope is part of the Australia Telescope which is funded by the Commonwealth of Australia for operation as a National Facility managed by CSIRO. FC is supported by NASA grant NAG 5-9950. DRL is a University Research Fellow funded by the Royal Society. MAM is an NSF MPS-DRF Fellow. VMK is a Canada Research Chair and is supported by NSERC, NATEQ and CIAR. IHS holds an NSERC University Faculty Award and is supported by a Discovery Grant.

REFERENCES

Camilo F., Kaspi V.M., Lyne A.G., Manchester R.N., Bell J.F., D'Amico N., McKay N.P.F., Crawford F., 2000, ApJ, 541, 367
Camilo F. et al., 2001a, ApJ, 557, L51
Camilo F. et al., 2001b, ApJ, 548, L187
Camilo F., Manchester R.N., Gaensler B.M., Lorimer D.R., 2002a, ApJ, 579, L25
Camilo F., Manchester R.N., Gaensler B.M., Lorimer D.R., Sarkissian J., 2002b, ApJ, 567, L71
Camilo F. et al., 2002, ApJ, 571, L41
Clifton T.R., Lyne A.G., Jones A.W., McKenna J., Ashworth M., 1992, MNRAS, 254, 177
Cordes J.M., Lazio J.T.W., 1997, ApJ, 475, 557
Cordes J.M., Lazio T.J.W., 2002, preprint (astro-ph/0207156)
Crawford F., 2000, PhD thesis, Massachusetts Institute of Technology
Crawford F., Kaspi V.M., Manchester R.N., Lyne A.G., Camilo F., D'Amico N., 2001, ApJ, 553, 367
Crawford F., Pivovaroff M.J., Kaspi V.M., Manchester R.N., 2002, in Patrick O. Slane, Bryan M. Gaensler, eds, ASP Conf. Ser. Vol. 271, Neutron Stars in Supernova Remnants. Astron. Soc. Pac., San Francisco, p. 37
D'Amico N., Stappers B.W., Bailes M., Martin C.E., Bell J.F., Lyne A.G., Manchester R.N., 1998, MNRAS, 297, 28
D'Amico N. et al., 2001, ApJ, 552, L45
Doherty M., Johnston S., Green A.J., Roberts M.S.E., Romani R.W., Gaensler B.M., Crawford F., 2003, MNRAS, 339, 1048
Edwards R.T., Bailes M., 2001, ApJ, 801, 553
Edwards R.T., Bailes M., van Straten W., Britton M.C., 2001, MNRAS, 326, 358
Faulkner A. et al., 2003, in Bailes M., Nice D., Thorsett S., Bailes M., eds, ASP Conf. Ser., Radio Pulsars, in press
Fierro J.M. et al., 1993, ApJ, 413, L27
Georgelin Y.M., Georgelin Y.P., 1976, A&A, 49, 57
Gonthier P.L., Ouellette M.S., Berrier J., O'Brien S., Harding A.K., 2002, ApJ, 565, 482
Green A.J., Cram L.E., Large M.I., Ye T., 1999, ApJS, 122, 207
Halpern J.P., Camilo F., Gotthelf E.V., Helfand D.J., Kramer M., Lyne A.G., Leighly K.M., Eracleous M., 2001, ApJ, 552, L125
Halpern J.P., Gotthelf E.V., Mirabal N., Camilo F., 2002, ApJ, 573, L41
Hartman R.C. et al., 1999, ApJS, 123, 79
Hobbs G. et al., 2002, MNRAS, 333, L7
Hulse R.A., Taylor J.H., 1974, ApJ, 191, L59
Johnston S., Manchester R.N., Lyne A.G., Bailes M., Kaspi V.M., Qiao G., D'Amico N., 1992, ApJ, 387, L37
Kaspi V.M., Manchester R.N., Johnston S., Lyne A.G., D'Amico N., 1996, AJ, 111, 2028
Kaspi V.M., Bailes M., Manchester R.N., Stappers B.W., Sandhu J.S., Navarro J., D'Amico N., 1997, ApJ, 485, 820
Kaspi V.M., Lackey J.R., Mattox J., Manchester R.N., Bailes M., Pace R., 2000a, ApJ, 528, 445
Kaspi V.M. et al., 2000b, ApJ, 543, 321
Kramer M., Xilouris K.M., Lorimer D.R., Doroshenko O., Jessner A., Wielebinski R., Wolszczan A., Camilo F., 1998, ApJ, 501, 270
Kramer M., Klein B., Lorimer D.R., Müller P., Jessner A., Wielebinski R., 2000, in Kramer M., Wex N., Wielebinski R., eds, IAU Coll. 177, Pulsar Astronomy – 2000 and Beyond. Astron. Soc. Pac., San Francisco, p. 37
Kuiper L., Hermsen W., Verbunt F., Lyne A.G., Stairs I.H., Thompson D.J., Cusumano G., 2000, in Kramer M., Wex N., Wielebinski R., eds, IAU Coll. 177, Pulsar Astronomy – 2000 and Beyond. Astron. Soc. Pac., San Francisco, p. 355
Kulkarni S.R., Clifton T.R., Backer D.C., Foster R.S., Fruchter A.S., Taylor J.H., 1988, Nat, 331, 50
Kuzmin A.D., Losovskii B.Y., 1997, Astron. Lett., 23, 283
Large M.I., Vaughan A.E., Mills B.Y., 1968, Nat, 220, 340
Lorimer D.R., Lyne A.G., Camilo F., 1998, A&A, 331, 1002
Lyne A.G., Lorimer D.R., 1994, Nat, 369, 127
Lyne A.G. et al., 2000, MNRAS, 312, 698
Malofeev V.M., Malov O.I., 1997, Nat, 389, 697
Manchester R.N., 1996, in Johnston S., Walker M.A., Bailes M., eds, IAU Coll. 160, ASP Conf. Ser. Vol. 105, Pulsars, Problems and Progress. Astron. Soc. Pac., San Francisco, 193
Manchester R.N., Lyne A.G., Taylor J.H., Durdin J.M., Large M.I., Little A.G., 1978, MNRAS, 185, 409
Manchester R.N., D'Amico N., Tuohy I.R., 1985, MNRAS, 212, 975
Manchester R.N., Mar D., Lyne A.G., Kaspi V.M., Johnston S., 1993, ApJ, 403, L29
Manchester R.N. et al., 2001, MNRAS, 328, 17 (Paper I)
Manchester R.N. et al., 2002, in Patrick O. Slane, Bryan M. Gaensler, eds, ASP Conf. Ser. Vol. 271, Neutron Stars in Supernova Remnants. Astron. Soc. Pac., San Francisco, p. 31
Maron O., Kijak J., Kramer M., Wielebinski R., 2000, A&AS, 147, 195
McLaughlin M.A., Cordes J.M., 2000, ApJ, 538, 818
McLaughlin M.A., 2001, PhD thesis, Cornell Univ.
McLaughlin M.A., Mattox J.R., Cordes J.M., Thompson D.J., 1996, ApJ, 473, 763

McLaughlin M.A., Cordes J.M., Hankins T.H., Moffett D.A., 1999, ApJ, 512, 929
Merck M. et al., 1996, A&AS, 120, 465
Morris D.J. et al., 2002, MNRAS, 335, 275 (Paper II)
Ramanamurthy P.V. et al., 1995, ApJ, 447, L109
Roberts M.S.E., Romani R.W., Johnston S., Green A.J., 1999, ApJ, 515, 712
Roberts M.S.E., Romani R.W., Johnston S., 2001, ApJ, 561, L187
Roberts M.S.E., Hessels J.W.T., Ransom S.M., Kaspi V.M., Freire P.C.C., Crawford F., Lorimer D.R., 2002, ApJ, 577, L19
Shemar S.L., Lyne A.G., 1996, MNRAS, 282, 677
Slane P., Gaensler B.M., Dame T.M., Hughes J.P., Plucinsky P.P., Green A., 1999, ApJ, 525, 357
Staelin D.H., Reifenstein E.C., III, 1968, Sci, 162, 1481
Stairs I.H. et al., 2001, MNRAS, 325, 979
Staveley-Smith L. et al., 1996, PASA, 13, 243
Sturner S.J., Dermer C.D., 1995, A&A, 293, L17
Taylor J.H., Cordes J.M., 1993, ApJ, 411, 674 (TC93)
Thompson D.J. et al., 1992, Nat, 359, 615
Torres D.F., Butt Y.M., Camilo F., 2001, ApJ, 560, L155
Wang N., Manchester R.N., Pace R., Bailes M., Kaspi V.M., Stappers B.W., Lyne A.G., 2000, MNRAS, 317, 843
Wolszczan A., Cordes J.M., Dewey R.J., 1991, ApJ, 372, L99
Zhang L., Zhang Y.J., Cheng K.S., 2000, A&A, 357, 957

This paper has been typeset from a TEX/LATEX file prepared by the author.